Simultaneous mRNA and protein quantification at the single-cell level delineates trajectories of CD4^{+} T-cell differentiation

Dominik Trzupek[1], Melanie Dunstan[1], Antony J. Cutler[1], Mercede Lee[1], Leila Godfrey[1], Dominik Aschenbrenner[2], Holm H. Uhlig[2], Linda S. Wicker[1], John A. Todd[1*] and Ricardo C. Ferreira[1*]

[1]JDRF/Wellcome Diabetes and Inflammation Laboratory, Wellcome Centre for Human Genetics, Nuffield Department of Medicine, NIHR Oxford Biomedical Research Centre, University of Oxford, Oxford, UK.
[2]Translational Gastroenterology Unit and Department of Paediatrics, John Radcliffe Hospital, University of Oxford, UK.

*Co-senior authors:

Correspondence:

Prof. John A. Todd:

Email: john.todd@well.ox.ac.uk

Dr. Ricardo C. Ferreira:

Email: ricardo.ferreira@well.ox.ac.uk

Abstract

The transcriptomic and proteomic characterisation of $CD4^+$ T cells at the single-cell level has been performed traditionally by two largely exclusive types of technologies: single cell RNA-sequencing (scRNA-seq) technologies and antibody-based cytometry. Here we demonstrate that the simultaneous targeted quantification of mRNA and protein expression in single-cells provides a high-resolution map of human primary $CD4^+$ T cells, and reveals precise trajectories of canonical T-cell lineage differentiation in blood and tissue. We report modest correlation between mRNA and protein in primary $CD4^+$ T cells at the single-cell level, highlighting the importance of including quantitative protein expression data to characterise cell effector function. This approach provides a massively-parallel, cost-effective, solution to dissect the heterogeneity of immune cell populations and is ideally suited for the detailed immunophenotypic characterisation of rare and potentially pathogenic immune subsets. This transcriptomic and proteomic hybrid technology could have important clinical applications to re-define differentiation and activation of tissue-resident and blood human immune cells.

Keywords: single-cell RNA-sequencing (scRNA-seq); AbSeq; immunophenotyping; primary $CD4^+$ T cell; human.

Introduction

Our understanding of the human immune system has been greatly influenced by the technological advances leading to the ability to precisely quantify mRNA and/or protein expression at the single-cell level. In particular, the implementation of flow cytometry as a routine and widely-accessible research tool has shaped much of our current knowledge about the complexity of the immune system. With increased availability of fluorochrome-conjugated antibodies and more powerful lasers, flow-cytometric assays allow typically 15-20 parameters that can be assessed in parallel. Developments in single-cell mass cytometry (CyTOF) have similarly allowed the simultaneous assessment of the expression of up to 50 protein targets using heavy metal-labeled antibodies[1].

The advent of single-cell RNA-sequencing (scRNA-seq) has provided an unprecedented opportunity to investigate the global transcriptional profile at the single-cell level. In contrast to cytometry-based technologies, which are limited to the concurrent detection of up to a few tens of protein markers, scRNA-seq technologies allow to profile the entire transcriptome. With the concomitant reduction in sequencing costs, there has been a recent explosion in scRNA-seq platforms available to immunologists[2,3]. These fundamentally differ in the cell capture methods and resulting sensitivity, ranging from a few hundreds of cells profiled with high sensitivity, using plate-based capture methods such as SMART-seq2[4], tens of thousands of cells with lower sensitivity using whole-transcriptome scRNA-seq platforms, such as 10X Genomics[5], Seq-Well[6] or Drop-seq[7].

Despite the growing popularity of whole-transcriptome scRNA-seq, two main issues still affect the performance of these platforms: cost and sensitivity. Even at high sequencing coverage, resulting in increased sequencing costs, stochastic dropout is a well-known issue of scRNA-seq, leading to an inflation of zero-expression measurements. Furthermore, although several methods have been developed to impute missing expression values, questions remain about the performance of these methods[8]. This technical limitation is particularly relevant for resting primary cells, such as $CD4^+$ T cells, and mainly limits the robust detection and quantification of

lowly expressed genes, including lineage-defining transcription factors, which are critical for cell-type identification and annotation.

In this study we describe an integrated workflow, using the BD Rhapsody targeted scRNA-seq system (commercialised by BD Biosciences), to simultaneously quantify the expression of 397 genes at the mRNA level and up to 68 genes at the protein level with oligo-conjugated antibodies (AbSeq). We sought to assess the sensitivity of this multi-omics system to immunophenotype human primary $CD4^+$ T cells at the single-cell level, and to identify discrete cell-states providing potential new insight into the functional heterogeneity of T cells. By combining the expression of a targeted set of genes with the highly quantitative measurement of key protein markers, we generated a high-resolution map of human $CD4^+$ T cells in blood and tissue, and delineated distinct trajectories of T-cell differentiation associated with a gradient of activation, which were apparent even in resting primary cells. Our data also shows very clearly the frequent low correlation between mRNA and protein expression in primary $CD4^+$ T cells, thereby challenging the current dogma that our current understanding of the immune system can be re-defined based on single-cell transcriptional data alone.

Results

Simultaneous protein quantification increases the power of scRNA-seq to dissect the functional heterogeneity of human CD4$^+$ T cells

In this study we wanted to investigate the power of a unified high-throughput experimental workflow combining targeted scRNA-seq and the quantification of protein expression at the single-cell level to dissect the heterogeneity of resting human primary CD4$^+$ T cells in blood. To address this question, we initially profiled the expression of 397 genes at the mRNA level, coupled with 37 protein targets (**Supplementary Table 1**) using the AbSeq technology[9] in CD4$^+$ T cells isolated from blood of a systemic lupus erythematosus (SLE) patient. To enrich for the relative distribution of two less abundant CD4$^+$ T-cell subsets: (i) CD127^{low}CD25$^+$ T cells, containing the Treg population; and (ii) CD127^{low}CD25^{low} T cells, containing a subset of non-conventional CD25^{low}FOXP3$^+$ Tregs previously characterised in autoimmune patients[10], we devised a FACS-sorting strategy to isolate and profile equal numbers of cells from the three defined T-cell subsets (**Fig. 1a**). Following FACS sorting, cells from each subset were labeled with a barcoded oligo-tagged antibody (sample tag) prior to cell loading – a method related to the recently described cell-hashing technique[11] – to identify their original sorting gate and to assess the frequency of cell multiplets obtained in this experiment.

A total of 9,898 captured cells passed initial QC, of which a small proportion (1.9%; **Supplementary Table 2**) were assigned as multiplets and excluded from the analysis. Of note, we observed complete sequencing saturation of the mRNA library, assessed as the number of cDNA molecules with a novel Unique Molecular Identifier (UMI) identified with increasing sequencing coverage, for a coverage of <3,000 reads/cell (**Supplementary Fig. 1a**). In contrast, we obtained an 80% sequencing saturation at a coverage of >6,000 reads/cell for the AbSeq library (**Supplementary Fig. 1b**). This is illustrated in the large dynamic range of expression of the protein targets, reaching up to thousands of unique copies in cells displaying higher levels of expression (**Supplementary Fig. 1c**). Of note, the distribution of most proteins, including all those that are known not to be expressed on CD4$^+$ T cells was centered around zero copies (**Supplementary Fig. 1c**), which demonstrates the high specificity of the AbSeq immunostainings. To further test the sensitivity of the AbSeq protein measurements, we next

generated a two-dimensional plot depicting the AbSeq expression of IL-2RA (CD25) and IL-7R (CD127), which we found to recapitulate the flow cytometric profile obtained with the same two markers used for the FACS-sorting of the assessed T-cell subsets (**Fig. 1b**). Furthermore, by overlaying the sample-tag information, we were able to confirm that the expression profiles of CD127 and CD25 mimicked the sorting strategy precisely for all three subsets (**Fig. 1b**), therefore illustrating the highly quantitative nature of the protein measurements.

Next we performed unsupervised hierarchical clustering combining the mRNA and protein expression data and visualised the clusters in a two-dimensional space using Uniform Manifold Approximation and Projection (UMAP)[12]. One of the main drivers of functional differentiation in $CD4^+$ T cells is the acquisition of a memory phenotype in response to antigen stimulation, typically marked by the expression of CD45RA on naïve cells and CD45RO on memory cells. However, because these are splice forms of the same gene (*PTPRC*; CD45), its discrimination cannot be achieved using UMI-based scRNA-seq systems targeting the 3' or 5' ends of the transcript. By measuring the expression of the two isoforms at the protein level, we were able to identify a marked expression gradient associated with a gradual loss of CD45RA and concomitant gain of CD45RO along the first component of the UMAP plot, indicating that the acquisition of a memory phenotype is indeed the main source of biological variation driving the clustering of $CD4^+$ T cells (**Fig. 1c**). One notable exception was the re-expression of CD45RA in the most differentiated memory cells (**Fig. 1c**). This observation is consistent with the phenotype of differentiated effector memory $CD4^+$ T cells that re-express CD45RA (TEMRAs)[13], and illustrates the power of this highly multiparametric approach to identify subtle alterations in $CD4^+$ T-cell states, while mitigating the potential issue of cell-type misclassification based on a few prototypical markers such as CD45RA/RO.

Single-cell mRNA and protein immunophenotyping identifies distinct trajectories of $CD4^+$ T cell differentiation in blood

Integration of the multiparametric transcriptional and proteomics data generated provided distinct clustering of $CD4^+$ T cells into discrete clusters along the naïve/memory differentiation axis (**Fig. 2a**). We observed an increased number of clusters within the memory compartment,

marked by the differential expression of defined sets of signature genes (**Fig. 2b** and **Supplementary Fig. 2a**), which was consistent with the increased phenotypic diversity in differentiated $CD4^+$ T-cell subsets. Moreover, we observed that the expression of the canonical Th1 (*TBX21*, encoding TBET) and Th17 (*RORC*, encoding RORγt) lineage-defining transcription factors was restricted to specific clusters within the memory effector T-cell (mTeff) population (**Fig. 2c**), indicating that these clusters are highly enriched for Th1 and Th17 Teffs. More importantly, similarly to the profile of CD45RA/RO expression, we observed a distinct gradient of expression of these transcription factors. Consistent with this gradient of functional differentiation, we observed a marked co-expression of canonical Th1 effector-type molecules with the expression of TBET (**Fig. 2d**), revealing a subset of highly activated Th1 T cells with a putative cytotoxic profile in the blood of this SLE patient. These data illustrate not only the sensitivity of the targeted scRNA-seq approach to sensitively quantify lowly expressed transcription factor genes, but also highlight the power of this integrated multi-omics approach to reveal trajectories of T-cell differentiation, which could be identified even in resting human primary $CD4^+$ T cells.

In addition to resting $CD4^+$ T cells, we also profiled the same subsets of cells following short *in vitro* stimulation (90 min) with PMA+ionomycin, to assess cell-type specific cytokine production. Similarly to the resting condition, *in vitro* stimulated $CD4^+$ T cells formed discrete clusters along the naïve-memory differentiation axis (**Supplementary Fig. 3a,b**). Furthermore, we observed a consistent induction of expression of Th1 (IFNγ) and Th17 (IL-22) type cytokines that were restricted to the respective Th1 and Th17 clusters (**Supplementary Fig 3c,d**). Furthermore, although primers for the Th2 transcription factor GATA-3 were not included in this assay, therefore precluding the annotation of Th2 cells in resting $CD4^+$ T cells, we noted that *in vitro* stimulation revealed a distinct cluster of Th2 mTeffs cells marked by the expression of Th2-type cytokines, such as IL-13 (**Supplementary Fig 3e**), but also IL-4, IL-5 and IL-9 (**Supplementary Fig. 2b**).

Targeted scRNA-seq and protein quantification reveals trajectories of human regulatory T cell activation in blood

Recently, several scRNA-seq studies have refined our understanding of the heterogeneity of $CD4^+$ Tregs and their functional adaptation in tissues, in both mice and humans[14,15]. Given the sorting strategy used in this study, we were able to significantly enrich our $CD4^+$ T-cell dataset for the Treg population, which is highly enriched within the $CD127^{low}CD25^{hi}$ population. Consistent with this enrichment strategy, we identified a large Treg population marked by the expression of the transcription factor FOXP3, but also other classical Treg signature genes, including HELIOS (encoded by *IKZF2*), IL-2RA, CTLA-4 or TIGIT (**Fig. 3a,b**). In agreement with their Treg-specific transcriptional programme, we found a marked suppression of IL-2 transcription in Tregs following *in vitro* stimulation (**Supplementary Fig. 3f**). Notably, we found that the differentiation of Tregs from a naïve to memory phenotype was strongly associated with the expression of two transcription factors: BACH2 and BLIMP1 (encoded by *PRDM1*). These two key transcription factors displayed a very distinct mutually exclusive expression pattern, with high expression of *BACH2* in naïve cells, declining gradually – with concomitant gradual increase in *PRDM1* expression – along the naïve-memory differentiation axis (**Fig. 3c**). The gradual increase of *PRDM1* expression was found to be strongly associated with the expression of Treg activation markers such as *HLA-DRA*, *DUSP4* and *CD39* (**Fig. 3d**), and revealed a trajectory of Treg activation in resting primary $CD4^+$ T cells. These data suggest that the transcriptional interplay between BACH2 and BLIMP-1 is critical to regulate the differentiation of memory Treg subsets, which is in agreement with previous data in both mouse and humans[14]. The dynamic interplay of *BACH2* and *PRDM1* in the differentiation of Tregs was even more pronounced following *in vitro* stimulation (**Supplementary Fig. 4**), which further supports the hypothesis that they are primary regulators of the transcriptional programme associated with the differentiation of suppressive activated Tregs in humans in response to antigen stimulation.

Multimodal immunophenotyping approach identifies rare populations of $CD4^+$ T cells in circulation

A feature of the most activated Treg cluster (cluster 3), was the marked differential expression of CD80 and CD86 at the protein level (**Fig. 3b,d**), two costimulatory molecules usually expressed in antigen presenting cells (APCs). Consistent with this restricted APC expression pattern, we

observed virtually no detectable expression of either *CD80* or *CD86* at the mRNA level in either resting or stimulated $CD4^+$ T cell (**Supplementary Fig. 5a,b**). Recently, a mechanism of transendocytosis of CD80/86 mediated by CTLA-4 has been described in mouse Tregs[16]. Therefore, one hypothesis is that the detected expression of these co-stimulatory molecules could be due to exogenous CD80/86 molecules captured by CTLA-4 expressed on activated Tregs from the surface of APCs. In support of this hypothesis, we observe that the expression of CD80/CD86 is specifically detected in the most activated Treg subset, which is also marked by high expression of CTLA-4 and HLA-class II molecules (**Fig. 3d**). To validate this observation, we next assessed the co-expression of CTLA-4 and CD80/86 by flow cytometry in $CD4^+$ T cells isolated from blood of two healthy donors. Although the expression of CTLA-4 on the surface of $CD4^+$ T cells is very low, intracellular staining revealed much higher expression on all Treg subsets (**Supplementary Fig. 5c,d**). In addition, we found that expression of CD86 and, to a lesser extent, CD80 were restricted to the memory Treg subset, and specifically to cells expressing the higher levels of CTLA-4 (**Supplementary Fig. 5e,f**). This striking co-expression of CD86 and CTLA-4 was particularly evident within a subset of $FOXP3^+HELIOS^-$ memory Tregs that expressed the higher levels of CTLA-4, and supports the hypothesis that these co-stimulatory molecules can be transiently detected on the surface of activated $CD4^+$ T cells. Furthermore, we also observe a strong co-expression of CD86 and HLA-DR, another marker associated with Treg activation (**Supplementary Fig. 5g**). We, however, cannot rule out that the possibility that CD80/CD86 is specifically expressed in activated $CD4^+$ T cells, but that the mRNA has a very short half-life, a hypothesis that has been previously reported[17]. We do note that the residual expression of CD80 and CD86 in both resting and *in vitro* stimulated $CD4^+$ T cells is mostly restricted to the activated Treg and memory Teff clusters (**Supplementary Fig. 5a,b**), and therefore, it is plausible that the expression of these co-stimulatory molecules in $CD4^+$ T cells is temporally restricted, while the protein expression is much more stable. Furthermore, we also note that expression of CD80 was strongly upregulated in Th17 Teffs (cluster 7; **Fig. 2b**), which may provide a mechanistic rationale for the recently reported suppression of Th17 differentiation in response to anti-CD80 treatment in mice[18]. Therefore, our data demonstrate the high sensitivity and specificity of the protein quantification using AbSeq, even using large numbers of antibodies simultaneously, and indicate that the surface expression of CD80 and

CD86 can be used to identify activated Tregs and Th17 cells in circulation, and further investigate the putative function of CD80/86 in $CD4^+$ T cells.

In addition, we were also able to identify a rare population of $FOXP3^+$ T cells marked by the specific expression of the small intestine-homing chemokine receptor CCR9 (cluster 10; **Fig. 3e**). This cluster was also marked by increased expression of other classical markers of tissue residency and migration to the gut, such as *ITGA4* (CD49d) and *ITGAE* (CD103; **Fig. 3e**). One distinguishing feature of this subset was the expression of the transcription factor *POU2AF1* (**Fig. 3e**). Interestingly, although *POU2AF1* (encoding OCA-B), has been mainly characterised as a B-cell specific transcription factor in blood, where it plays a role in B-cell maturation[19], it has also been recently shown in mice to regulate the maintenance of memory phenotype and function in previously activated $CD4^+$ T cells[20], and the differentiation of T follicular helper (Tfh) cells in the tissue[21]. These data suggest that this subset of $CCR9^+$ T cells may represent a previously uncharacterised population of recirculating tissue-resident Tregs in humans, and provides an illustrative example of the power of this multiparametric immunophenotyping approach to identify rare populations of $CD4^+$ T cells.

Data from independent experiments can be robustly integrated

Given that the main advantage of this combined targeted scRNA-seq and proteomic approach is the ability to immunophenotype large numbers of cells from multiple donors, we next investigated whether we were able to integrate data generated from independent experiments. We replicated the initial experiment using the same pre-sorting strategy to isolate the three assessed $CD4^+$ T-cell subsets from an individual with type 1 diabetes and one healthy donor. To further test the limits of the protein quantification, we extended the AbSeq panel to 43 protein targets expressed on $CD4^+$ T cells (**Supplementary Table 1**). In agreement with the initial experiment, unsupervised clustering of the 23,947 cells passing QC revealed a similar discrimination of $CD4^+$ T-cell subsets (**Fig. 4a**). More importantly, we found very good alignment of the data from the three donors, with minimal evidence of significant experimental batch effects (**Fig. 4b**).

Furthermore, analysis of the donor-specific distribution of the identified $CD4^+$ T-cell clusters showed that the frequency of the putative $CD4^+$ cytotoxic Th1 subset (cluster 11), marked by the co-expression of TBET and effector-type cytokines, was highly increased in the SLE patient (**Fig. 4c-e**). To avoid age-specific differences in the relative distribution of the $CD45RA^+$ naïve and $CD45RO^+$ memory compartments in these donors, we normalised the analysis to the memory T-cell clusters only, which we were able to robustly annotate using the AbSeq data for the expression of CD45RA and CD45RO. Although we detected a few cells with this activated Th1 phenotype in circulation from every donor, there was a very substantial expansion in the SLE patient (2.3% of memory $CD4^+$ T cells compared to 0.3% and 0.1% in the T1D patient and healthy donor, respectively; **Fig. 4d**), suggesting that it could represent a pathogenic $CD4^+$ T-cell subset associated with systemic autoimmunity in this patient.

Single-cell comparison of mRNA and protein expression levels reveals modest and variable levels of correlation in primary $CD4^+$ T cells

The parallel quantification of mRNA and protein expression for a large number of genes expressed in $CD4^+$ T cells in this experiment provided a unique opportunity to investigate their systematic correlation at the single-cell level. From the 43 proteins quantified with AbSeq, 26 were also assessed at the transcriptional level and detected in our $CD4^+$ T-cell dataset. Generally, we observed modest (median Pearson correlation coefficient = 0.183) but variable levels of correlation in total resting $CD4^+$ T cells, ranging from 0.039 for *TNFRSF9* to 0.808 in *KLRB1* (encoding CD161; **Fig. 5a**). These findings were consistent with previous observations[22,23], and suggest that primary $CD4^+$ T cells are highly specialised cells, where transcription is subject to tight regulation to avoid excessive energy consumption by the cell and to control effector function. As expected, by normalizing our analysis to a functionally more homogeneous population of memory $CD4^+$ T cells, we observed higher levels of correlation, which is consistent with their increased expression of the majority of the assessed T-cell markers. A slightly decreased correlation (median = 13.9%) was observed in *in vitro* stimulated $CD4^+$ T cells, suggesting an increased variance of protein and mRNA expression in activated $CD4^+$ T cells (**Fig. 5b**).

Parallel mRNA and protein profiling provides increased cell-type resolution of the heterogeneous CD45$^+$ immune cell population in blood and tissue

To investigate how this combined targeted scRNA-seq and transcriptomics approach performs on a more heterogeneous population of immune cells, we isolated total CD45$^+$ cells isolated from blood and a matching duodenal biopsy from two pediatric coeliac disease (CD) patients with active disease. In this experiment we captured a total of 31,907 single-cells that passed QC and expanded the AbSeq panel to the detection of 68 protein targets (**Supplementary Table 1**). As expected, we observed a very defined clustering of the different cell populations representing the CD45$^+$ immune cells (**Fig. 6a**). Consistent with previous data[24,25], we found a clear separation in cells isolated from either blood or the small intestine (**Fig. 6b**), indicating a strong transcriptional signature of tissue-residency. Furthermore, clustering of the cells isolated from either blood (**Fig. 6c**) and tissue (**Fig. 6d**) separately, revealed clear identification of the expected cell populations in both tissues, which could be easily manually annotated based on the differential expression of canonical cell-type specific gene signatures. The main distinction was the relative distribution of the main immune populations, with a marked increased representation of B-cell, NK-cell and undifferentiated CD14$^+$CD16$^-$ monocyte populations in blood, and a significant increase in the frequency of plasma cells in the small intestine. We were similarly able to similarly identify distinct trajectories of cell differentiation in other immune cell subsets, as illustrated by the gradient of differentiation and class-switching of B cells in blood (**Supplementary Fig. 6a-c**). B cells in circulation were clearly dominated by a naïve IgD$^+$IgM$^+$ CD27$^-$ subset, and only a small fraction of class-switched IgG$^+$ CD27$^+$ memory B cells, which was consistent with the young age of the CD patients. In contrast, in the small intestine, we observed only a small population of B cells, which were mostly represented by the class switched IgG$^+$ CD27$^+$ memory phenotype. In addition, we identified a vastly expanded population of antibody-secreting plasma cells (**Supplementary Fig 6d,e**). Of note, because we were able to specifically assess the expression of the secreted Ig isotypes, we could also discriminate precisely the different functional plasma cell subsets, including a very abundant population IgA-secreting plasma cells (**Supplementary Fig. 6f**), which are known play a critical role in interaction with the microbiome in the gut.

In agreement with our findings in $CD4^+$ T cells, we found that the acquisition of a memory phenotype was the main driver of the clustering of both $CD4^+$ and $CD8^+$ T cells (**Supplementary Fig. 7a,b**). In addition, we were also able to identify other clusters of non-conventional T cells, including a subset of γt T cells and mucosal-associated invariant T cells (MAIT) in blood, which shared similarities with the transcriptional signature of memory $CD8^+$ T cells, marked by the expression of high levels of effector-type cytokines genes, such as *NKG7* (**Supplementary Fig. 7b**). In contrast, $CD4^+$ T cells isolated from the small intestine, consistent with their tissue-resident function, were restricted to a memory phenotype and displayed a higher level of functional heterogeneity (**Fig. 6e**). Notably, we identified a very enlarged population of $FOXP3^+$ Tregs in the tissue compared to the matching circulating subset (**Fig. 6f**). Moreover, the simultaneous assessment of the protein expression of CXCR5, ICOS and PD-1, identified a cluster of Tfh cells, which could be distinctly clustered along a trajectory of Tfh-cell activation, as illustrated by the gradient of expression of key Tfh functional transcripts, such as *IL21*, *CXCL13* and *BTLA* (**Fig. 6g,h**). Together, these data provide an example of the power of this multimodal approach to identify trajectories of cell differentiation and cell states in diverse immune cell and tissue types.

Discussion

The advent of scRNA-seq has proved to be a transformative technology that is shaping our understanding of the complexity and function of the human immune system[26,27]. However, currently, both the elevated costs to perform these experiments, as well as the reliance on transcriptional data alone, pose significant challenges to the widespread practical applicability of these technologies. In this study, we present an integrated, cost-effective, approach to sensitively assess simultaneous expression of mRNA and protein for hundreds of key immune targets at the single-cell level using the AbSeq technology[9].

Recently, two similar approaches, CITE-seq[22] and REAP-seq[23], have been described to measure protein expression using oligo-tagged antibodies in parallel with scRNA-seq data. Furthermore, other applications are currently being developed to integrate the growing portfolio of single-cell omics technologies[28]. A fundamental difference with the approach described in this study is that these technologies all rely on whole-transcriptome data, providing a high-level cross-sectional representation of all polyA transcripts in the cell. In contrast, by using targeted scRNA-seq, we are relying on prior knowledge to specifically assess the expression of hundreds of selected genes in single cells. A limitation of this approach is that it is, by definition, restricted to the set of pre-selected genes, and therefore is not suited for a purely discovery-based exploratory experiment, where the identification of novel biological determinants of cellular identity is the central question – particularly in poorly characterised non-immune cell types. However, as the transcriptome of immune cell subsets becomes better characterised, it may become feasible to target the expression of the most variable genes, which could yield novel insight into previously uncharacterised biology and regulation. Moreover, a targeted approach provides a more sensitive quantification of expression of the selected genes at a fraction of the cost to generate the sequencing libraries, as it avoids the detection of highly expressed invariant housekeeping genes, which take up the vast majority of the whole-transcriptome scRNA-seq libraries. The increased sensitivity of a targeted approach is particularly relevant for the accurate assessment of lowly-expressed genes with critical regulatory function, such as transcription factors, which can be poorly quantified using traditional whole-transcriptome scRNA-seq data. It therefore, provides a knowledge-based approach to validate and extend whole-transcriptome scRNA-seq findings, that

can be widely implemented in any research or clinical setting. Similarly to other widely-implemented knowledge-based single-cell immunophenotyping tools such as flow-cytometry and CyTOF, the highly customisable nature of this approach is critical to investigate specific research questions with very high sensitivity and in larger number of samples. However, in contrast to CyTOF which is inherently time-consuming and requires the availability of very large numbers of cells to maximise the information generated by each run, this technology is ideally suited for unique and highly valuable clinical samples, for which cell availability and number are major practical constraints.

An important finding from this study and other related studies[22,23], is the generally low levels of correlation between mRNA and protein expression in primary $CD4^+$ T cells at the single-cell level. One possible explanation for this observation is that reduced sensitivity of scRNA-seq to quantify mRNA expression, may be leading to an underestimation of the correlation coefficients. However, we note that there are notable exceptions, such as CD161, which displayed a high correlation between mRNA and protein levels at 0.847 in memory $CD4^+$ T cells, demonstrating that a systematic error in the quantification of mRNA levels by scRNA-seq technologies is not the only factor contributing to the observed low level of correlation. These findings therefore underscore the importance of parallel protein quantification to better identify stable cellular phenotypes associated with cell function. In contrast to mRNA expression, proteins display a much larger dynamic range of expression and longer half-life[29,30], resulting in much higher copy numbers, and a more accurate and reliable quantification compared to their mRNA counterparts. This is particularly relevant in differentiated resting primary cells, such as $CD4^+$ T cells, where transcription is tightly regulated to maintain effector function. These low copy numbers result in increased stochastic variation in mRNA quantification and dropout rate, which impair the accuracy single-cell methods that rely only on transcriptional data. Furthermore, mRNA profiling provides only a snapshot into the current functional state of the cell, which can be better assessed with combined protein expression data. An illustration of the power of this combined multimodal approach is the detailed trajectories of differentiation that we identified in resting primary $CD4^+$ T cells, which were recapitulated by precise gradients of mRNA expression. The sensitivity of these measurements combined with the high numbers of cells analysed lend themselves to identify gradual and subtle changes in cell states, which are critical to identify

dynamic changes reflecting mechanisms of functional adaptation in a heterogeneous cell population.

The digital nature and lack of spectral overlap issues with the AbSeq measurements provide a superior specificity and sensitivity compared to flow cytometry for the quantification of lowly-expressed proteins, allowing accurate detection of zero or very low copy numbers, which are usually difficult to discriminate by flow cytometry. A good example was the sensitive quantification of the co-stimulatory protein CD80 by AbSeq, whose expression was found to be restricted to a cluster of activated Tregs and Th17 Teff cells. In comparison, flow cytometric assessment of CD80 expression was much less well-resolved with higher background, resulting in lower dynamic range of expression comparing to AbSeq. Currently, we have assessed the expression of up to 68 protein targets in parallel, with minimal evidence of sensitivity or specificity issues. There is no theoretical limit to the number of proteins that can be assessed in parallel, although the expression levels of the assessed target proteins may be the only major technical limitation. To date, protein quantification is restricted to surface-expressed targets, although as this technology develops, assessment of intracellular targets will further improve the scope of this approach. Furthermore, parallel detection of TCR and BCR sequences in this system is currently being developed[31], which will provide critical insight into the clonality of the assessed T- and B-cell subsets. This is particularly relevant in the field of autoimmune diseases as a new tool to identify the elusive pathogenic autoreactive cell clones.

In summary we here show that combined targeted scRNA-seq and protein expression analysis provides a high-resolution map of human primary $CD4^+$ T cells in blood and tissue, and reveals precise trajectories of functional differentiation. Our data provide a proof-of-principle for the implementation of this integrated approach as a widely applicable, and cost-efficient research tool for immunologists that could be particularly valuable in a clinical setting for the characterisation of rare patient samples with limited cell numbers, as well as to assess the functional consequence at the single-cell level of targeting key biological pathways *in vivo*, in patients treated with immunotherapeutic drugs.

Methods

Subjects

Study participants included one SLE patient (37 y/o female), recruited from the Cambridge BioResource, and one T1D patient (16 y/o male) and one autoantibody negative healthy donor (14 y/o male) recruited from the JDRF Diabetes–Genes, Autoimmunity and Prevention (D-GAP) study.

Comparison of total $CD45^+$ immune cells isolated from paired blood and a duodenal biopsy was performed in cells isolated from two paediatric coeliac disease (CD) patients with active disease (one 5 y/o male with Marsh scale disease score of 3c, and one 15 y/o male with Marsh scale disease score of 3b).

Flow cytometric assessment of the expression of CTLA-4, CD80 and CD86 in the Treg subsets was performed in two adult healthy donors (53 y/o female and 33 y/o male), recruited from the Oxford Biobank.

All samples and information were collected with written and signed informed consent. The study was approved by the local Peterborough and Fenland research ethics committee (05/Q0106/20). The D-GAP study was approved by the Royal Free Hospital & Medical School research ethics committee; REC (08/H0720/25). Small bowel biopsies were collected as part of a routine gastroduodenoscopy. Consent for research was obtained via the Oxford GI illnesses biobank (REC 16/YH/0247).

Cell preparation and FACS sorting

T-cell centric assays were performed on cryopreserved peripheral blood mononuclear cells (PBMCs). Cryopreserved PBMCs were thawed at 37°C and resuspended drop-by-drop in X-VIVO (Lonza) with 1% heat-inactivated, filtered human AB serum (Sigma). Total $CD4^+$ T cells were isolated by negative selection using magnetic beads (StemCell Technologies), and incubated with Fixable Viability Dye eFluor 780 (eBioscience) for 15 min at room temperature. After washing in PBS with 0.02% BSA cells were stained in 5ml FACS tubes (Falcon) with the fluorochrome-conjugated antibodies used for cell sorting and the BD AbSeq oligo-conjugated

antibodies (BD Bioscience), according to the manufacturer's instructions.

Cell sorting was performed using a BD FACSAria Fusion sorter (BD Biosciences) at 4ºC into 1.5 mL DNA low bind Eppendorf tubes containing 500ul of X-Vivo with 1% heat-inactivated, filtered human AB serum. Following cell sorting, the three assessed T-cell subsets were incubated with sample tag antibodies (Sample multiplexing kit; BD Bioscience), washed 3 times in cold BD sample buffer (BD Biosciences) and counted. Samples were then pooled together in equal ratios in 620 ul of cold BD sample buffer at the desired cell concentrations – ranging from 20 to 40 cells/ul for an estimated capture rate of 10,000-20,000 single-cells – and immediately loaded on a BD Rhapsody cartridge (BD Biosciences) for single-cell capture.

For the *in vitro* stimulated condition, sorted $CD4^+$ T-cell subsets were incubated in round-bottom 96-well plates (20,000 cells/well) at 37ºC for 90 min in X-Vivo with 5% heat-inactivated, filtered human AB serum with a PMA and ionomycin cell stimulation cocktail (eBioscience), in the absence of protein transport inhibitors. Cells were harvested into FACS tubes, washed with cold BD sample buffer and further incubated with the BD AbSeq oligo-conjugated antibodies, according to the manufacturer's instructions. All FACS/sorting and AbSeq antibodies used in this study are listed in **Supplementary Table 1**.

Tissue dissociation and isolation of $CD45^+$ immune cells

For the characterisation of $CD45^+$ immune cells from tissue and tissue, blood-derived PBMCs and paired duodenal biopsies were cryopreserved in CryoStor CS10 reagent (StemCell) and stored in liquid nitrogen until sample processing. Blood-derived PBMCs were processed as described above. The paired duodenal biopsies were thawed at 37ºC in X-Vivo with 1% heat-inactivated, filtered human AB serum then subjected to gentle mechanical dissociation using gentleMACS (Miltenyi Biotec) followed by short 20 min enzymatic dissociation at 37ºC using a very low concentration of Liberase TL (0.042 mg/ml; Sigma), 10 nM HEPES and 1mg/ml DNase I in X-Vivo with 10% FBS. Following enzymatic dissociation, the biopsies were homogenised using a more vigorous gentleMACS cycle and strained through a 70um filter with

physical maceration to generate single-cell suspensions. $CD45^+$ immune cells were further enriched using a 70/35% Percoll gradient (Sigma). The dissociation protocol and low concentration of Liberase TL enzyme were optimised to show minimal effect on the degradation of surface protein expression levels, as assessed by flow cytometry. This was critical to ensure maximal sensitivity and specificity of the AbSeq protein quantification in these samples.

Blood- and tissue-derived single-cell suspensions were incubated with Fixable Viability Dye eFluor 780 for 15 min at room temperature and total $CD45^+$ cells were isolated by FACS sorting. Following FACS sorting the individual blood and tissue-derived subsets were incubated with Fc block reagent (BD Biosciences) and Sample Tag antibodies for 20 min at room temperature. Following three rounds of washing, cells were counted and equal numbers (35,000 cells) of blood- and tissue-derived cells from the same donor were pooled together and incubated with AbSeq antibody mastermix (**Supplementary Table 1**) according to the manufacturer's instructions. Cells were then washed two times in cold sample buffer, counted and resuspended in 620 ul of cold sample Buffer at a final concentration of 40 cells/ul for loading on a BD Rhapsody cartridge.

cDNA library preparation and sequencing

Single-cell capture and cDNA library preparation was performed using the BD Rhapsody Express Single-cell analysis system (BD Biosciences), according to the manufacturer's instructions. Briefly, cDNA was amplified - 10 cycles for resting cells and 9 cycles for *in vitro* activated cells - using the Human Immune Response primer panel (BD Biosciences), containing 399 primer pairs, targeting 397 different genes. The resulting PCR1 products were purified using AMPure XP magnetic beads (Beckman Coulter) and the respective mRNA and AbSeq/Sample tag products were separated based on size-selection, using different bead ratios (0.7X and 1.2X, respectively). The purified mRNA and Sample tag PCR1 products were further amplified (10 cycles), and the resulting PCR2 products purified by size selection (1X and 1.2X for the mRNA and Sample tag libraries, respectively). The concentration, size and integrity of the resulting PCR products was assessed using both Qubit (High Sensitivity dsDNA kit; Thermo Fisher) and the Agilent 4200 Tapestation system (High Sensitivity D1000 screentape; Agilent). The final

products were normalised to 2.5 ng/ul (mRNA), 0.5 ng/ul (Sample tag) and 0.275 ng/ul (AbSeq) and underwent a final round of amplification (6 cycles for mRNA and 8 cycles for Sample Tag and AbSeq) using indexes for Illumina sequencing to prepare the final libraries. Final libraries were quantified using Qubit and Agilent Tapestation and pooled (~38/58/2% mRNA/AbSeq/Sample tag ratio) to achieve a final concentration of 5nM. Final pooled libraries were spiked with 10% PhiX control DNA to increase sequence complexity and sequenced (75bp paired-end) on HiSeq 4000 sequencer (Illumina).

CD80/86 immunophenotyping

Immunophenotyping of the co-stimulatory molecules CD80/CD86 and CTLA-4 was performed in both freshly isolated and cryopreserved PBMCs. Cells were initially stained with fluorochrome-conjugated antibodies against surface receptors (see **Supplementary Table 1**) in BD Brilliant stain buffer (BD Biosciences) for 30 min at room temperature. Fixation and permeabilisation was performed using FOXP3 Fix/Perm Buffer Set (eBioscience) according to the manufacturer's instructions, and cells were then immunostained with fluorochrome-conjugated antibodies against intracellular markers (including CTLA-4, CD80 and CD86 where indicated) in BD Brilliant stain buffer for 45 min at room temperature. Immunostained samples were acquired using a BD Fortessa (BD Biosciences) flow cytometer with FACSDiva software (BD Biosciences) and analysed using FlowJo (Tree Star, Inc.).

Data analysis and QC

The FASTQ files obtained from sequencing were analysed following the BD Biosciences Rhapsody pipeline (BD Biosciences). Initially, read pairs with low quality are removed based on read length, mean base quality score and highest single nucleotide frequency. The remaining high-quality R1 reads are analysed to identify cell label and unique molecular identifier (UMI) sequences. The remaining high-quality R2 reads are aligned to the reference panel sequences (mRNA and AbSeq) using Bowtie2. Reads with the same cell label, same UMI sequence and same gene are collapsed into a single molecule. The obtained counts are adjusted by BD Biosciences developed error correction algorithms – recursive substitution error correction (RSEC) and distribution-based error correction (DBEC) – to correct sequencing and PCR errors. Cell counts are then estimated, using second derivative analysis to filter out noise cell labels,

based on the assumption that putative cells have much more reads than noise cell labels. Thus when cells are sorted in the descending order by number of reads, the inflection point can be observed on a log transformed cumulative curve of number of reads. For the $CD45^+$ sorted cells, due to the heterogeneity of the sample, we observed two inflection points (and two corresponding second derivative minima), and therefore, only cell labels after the second inflection point were considered noise labels. Barcoded oligo-conjugated antibodies (single-cell multiplexing kit; BD Biosciences) were used to infer origin of sample (ie. sorted cell population) and multiplet rate by the BD Rhapsody analysis pipeline.

The DBEC-adjusted molecule counts obtained from the Rhapsody pipeline were imported and the expression matrices were further analysed using R package Seurat 3.0[32]. Most cells identified as undetermined by the Rhapsody pipeline had low number of features (mRNA and protein reads). These cells along with other cells with similarly low (<35) number of features were filtered out. Identified multiplet cells were also filtered out at this stage. A detailed summary of the number of putative captured cells, estimated multiplet rate and number of cells filtered from the analysis in each of the three experiments performed in this study is provided in **Supplementary Table 2**. The resulting matrices were log normalised using the default parameters in Seurat and the UMI counts were regressed out when scaling data. Uniform Manifold Approximation and Projection (UMAP) was used for dimensionality reduction. The default number of used dimensions of PCA reduction was increased to 30 based on Seurat elbow plot. For clustering, we increased the default resolution parameter value for clustering to 1.2 to obtain more fine-grained set of clusters. Differential expression analysis was performed using negative binomial generalized linear model implemented in Seurat, and integration of data from multiple experiments was performed using a combination of canonical correlation analysis (CCA) and identification of mutual nearest neighbours (MNN), implemented in Seurat 3.0 [33].

Acknowledgements

We thank donors and patients for participation in this study. We gratefully acknowledge the participation of all NIHR Cambridge BioResource volunteers, and thank the NIHR Cambridge BioResource centre and staff for their contribution. We thank C. Guy from the Department of Paediatrics, University of Cambridge for D-GAP sample recruitment. We thank the volunteers from the Oxford Biobank (www.oxfordbiobank.org.uk) for their participation in this recall study. The Oxford BioBank and Oxford Bioresource are funded by the NIHR Oxford Biomedical Research Centre (BRC). We acknowledge the contribution of the Oxford Gastrointestinal biobank, which is supported by the NIHR Oxford Biomedical Research Centre. We also thank Georgina Burdon, Shannah Donhou, Sarune Kacinskaite and Heather McMurray, University of Oxford for sample collection and preparation and members of the Diabetes and Inflammation Laboratory for critical discussion.

Funding

This work was supported by the JDRF UK Centre for Diabetes - Genes, Autoimmunity and Prevention (D-GAP; 4-2007-1003) in collaboration with M. Peakman and T. Tree at Kings College London, a strategic award to the Diabetes and Inflammation Laboratory from the JDRF (4-SRA-2017-473-A-A) and the Wellcome (107212/A/15/Z), and a grant from the JDRF (1-SRA-2019-657-A-N).

Conflict of interest

The authors report no conflict of interest.

References

1. Ornatsky, O. *et al.* Highly multiparametric analysis by mass cytometry. *J. Immunol. Methods* **361**, 1–20 (2010).
2. See, P., Lum, J., Chen, J. & Ginhoux, F. A Single-Cell Sequencing Guide for Immunologists. *Frontiers in Immunology* **9**, 2425 (2018).
3. Papalexi, E. & Satija, R. Single-cell RNA sequencing to explore immune cell heterogeneity. *Nat. Rev. Immunol.* **18**, 35 (2017).
4. Picelli, S. *et al.* Smart-seq2 for sensitive full-length transcriptome profiling in single cells. *Nat. Methods* **10**, 1096 (2013).
5. Zheng, G. X. Y. *et al.* Massively parallel digital transcriptional profiling of single cells. *Nat. Commun.* **8**, 14049 (2017).
6. Gierahn, T. M. *et al.* Seq-Well: portable, low-cost RNA sequencing of single cells at high throughput. *Nat. Methods* **14**, 395 (2017).
7. Macosko, E. Z. *et al.* Highly Parallel Genome-wide Expression Profiling of Individual Cells Using Nanoliter Droplets. *Cell* **161**, 1202–1214 (2015).
8. Andrews, T. S. & Hemberg, M. False signals induced by single-cell imputation. *F1000Research* **7**, (2018).
9. Shahi, P., Kim, S. C., Haliburton, J. R., Gartner, Z. J. & Abate, A. R. Abseq: Ultrahigh-throughput single cell protein profiling with droplet microfluidic barcoding. *Sci. Rep.* **7**, 44447 (2017).
10. Ferreira, R. C. *et al.* Cells with Treg-specific FOXP3 demethylation but low CD25 are prevalent in autoimmunity. *J. Autoimmun.* **84**, 75–86 (2017).
11. Stoeckius, M. *et al.* Cell Hashing with barcoded antibodies enables multiplexing and doublet detection for single cell genomics. *Genome Biol.* **19**, 224 (2018).
12. McInnes, L., Healy, J. & Melville, J. UMAP: Uniform Manifold Approximation and Projection for Dimension Reduction. *arXiv* **arXiv:1802**, (2018).
13. Sallusto, F., Lenig, D., Förster, R., Lipp, M. & Lanzavecchia, A. Two subsets of memory T lymphocytes with distinct homing potentials and effector functions. *Nature* **401**, 708–712 (1999).
14. Zemmour, D. *et al.* Single-cell gene expression reveals a landscape of regulatory T cell phenotypes shaped by the TCR. *Nat. Immunol.* **19**, 291–301 (2018).
15. Miragaia, R. J. *et al.* Single-Cell Transcriptomics of Regulatory T Cells Reveals Trajectories of Tissue Adaptation. *Immunity* **50**, 493-504.e7 (2019).
16. Ovcinnikovs, V. *et al.* CTLA-4–mediated transendocytosis of costimulatory molecules primarily targets migratory dendritic cells. *Sci. Immunol.* **4**, eaaw0902 (2019).
17. Höllsberg, P. *et al.* Expression of a hypoglycosylated form of CD86 (B7-2) on human T cells with altered binding properties to CD28 and CTLA-4. *J. Immunol.* **159**, 4799–4805 (1997).
18. Huang, Y., Li, Y., Wei, B., Wu, W. & Gao, X. CD80 Regulates Th17 Cell Differentiation in Coxsackie Virus B3-Induced Acute Myocarditis. *Inflammation* **41**, 232–239 (2018).
19. Schubart, D. B., Rolink, A., Kosco-Vilbois, M. H., Botteri, F. & Matthias, P. B-cell-specif ic coactivator OBF-1/OCA-B/Bob1 required for immune response and germinal centre formation. *Nature* **383**, 538–542 (1996).
20. Shakya, A. *et al.* Oct1 and OCA-B are selectively required for CD4 memory T cell function. *J. Exp. Med.* **212**, 2115–2131 (2015).
21. Stauss, D. *et al.* The transcriptional coactivator Bob1 promotes the development of

follicular T helper cells via Bcl6. *EMBO J.* **35**, 881–898 (2016).

22. Stoeckius, M. *et al.* Simultaneous epitope and transcriptome measurement in single cells. *Nat. Methods* **14**, 865 (2017).

23. Peterson, V. M. *et al.* Multiplexed quantification of proteins and transcripts in single cells. *Nat. Biotechnol.* **35**, 936 (2017).

24. Kumar, B. V *et al.* Human Tissue-Resident Memory T Cells Are Defined by Core Transcriptional and Functional Signatures in Lymphoid and Mucosal Sites. *Cell Rep.* **20**, 2921–2934 (2017).

25. Szabo, P. A. *et al.* A single-cell reference map for human blood and tissue T cell activation reveals functional states in health and disease. *bioRxiv* 555557 (2019).

26. Stubbington, M. J. T., Rozenblatt-Rosen, O., Regev, A. & Teichmann, S. A. Single-cell transcriptomics to explore the immune system in health and disease. *Science* **358**, 58–63 (2017).

27. Tanay, A. & Regev, A. Scaling single-cell genomics from phenomenology to mechanism. *Nature* **541**, 331 (2017).

28. Mimitou, E. P. *et al.* Multiplexed detection of proteins, transcriptomes, clonotypes and CRISPR perturbations in single cells. *Nat. Methods* **16**, 409–412 (2019).

29. Schwanhäusser, B. *et al.* Global quantification of mammalian gene expression control. *Nature* **473**, 337 (2011).

30. Vogel, C. & Marcotte, E. M. Insights into the regulation of protein abundance from proteomic and transcriptomic analyses. *Nat. Rev. Genet.* **13**, 227 (2012).

31. Chang, C., Nakamoto, M., Lai, J., Siddique, I. & Mortimer, S. Simultaneous mRNA, protein, and immune-repertoire profiling of thousands of single cells. *J. Immunol.* **202**, 131.40 (2019).

32. Butler, A., Hoffman, P., Smibert, P., Papalexi, E. & Satija, R. Integrating single-cell transcriptomic data across different conditions, technologies, and species. *Nat. Biotechnol.* **36**, 411 (2018).

33. Stuart, T. *et al.* Comprehensive Integration of Single-Cell Data. *Cell* **177**, 1888-1902.e21 (2019).

Figure legends

Figure 1. Integrated single-cell targeted multi-omics approach provides a high-resolution map of human primary CD4$^+$ T cells in blood. (**a**) Summary of the experimental workflow. FACS plot depicts the sorting strategy for the isolation of the three assessed CD4$^+$ T cell populations. (**b**) Two-dimensional plot depicting the IL-7R and IL-2RA expression at the protein level using oligo-tagged antibodies (AbSeq) on each captured single cell. Cells are colored according to their respective sorting gate, as assessed using oligo-conjugated sample-tagging antibodies. (**c**) UMAP (uniform manifold approximation projection) plot depicting the clustering of all captured CD4$^+$ single cells using the combined proteomics and transcriptomics data. Expression levels of the CD45RA (black to green) and CD45RO (black to red) isoforms using AbSeq antibodies is depicted in the plot for each cell. Arrow indicates the gradient of decreasing CD45RA and concomitant gain in CD45RO expression associated with the acquisition of a CD4$^+$ T-cell memory phenotype in response to antigen stimulation.

Figure 2. Combined single-cell transcriptional and proteomics immunophenotyping reveals distinct trajectories of CD4$^+$ T cell differentiation *in vivo*. (**a**) UMAP plot depicts the clustering of the resting primary CD4$^+$ T cells isolated from blood of a systemic lupus erythematosus (SLE) patient. (**b**) Heatmap depicts the top 10 differentially expressed genes in each identified resting CD4$^+$ Teff cluster. (**c**) UMAP plots depicting the expression of the CD4$^+$ T-cell lineage-defining transcription factors TBET (Th1) and RORγt (Th17) in resting CD4$^+$ T cells. Arrows indicate the gradient of the expression of the respective transcription factor, recapitulating the identified axis of CD4$^+$ lineage differentiation. (**d**) Expression of the effector-type cytokine transcripts *IFNγ, NKG7*, *PRF1*, *CCL5*, *GZMH* and *GZMK* in resting CD4$^+$ T cells.

Figure 3. Identification of a trajectory of human CD4$^+$ regulatory T cell (Treg) activation. (**a**) UMAP plot depicts the expression of the canonical Treg transcription factor FOXP3 in the identified resting CD4$^+$ T-cell clusters. (**b**) Heatmap depicts the top 10 differentially expressed genes within the four identified resting Treg clusters. (**c**) Plot depicts the overlaid expression of

two key $CD4^+$ T-cell transcription factor *BACH2* (black to green) and *PRDM1* (encoding BLIMP-1; black to red). (**d**) Illustrative example of the expression of highly differentially expressed genes within the cluster of activated Tregs (cluster 3), including *HLA-DRA* and *DUSP4* at the mRNA level and CD39, CCR4, CD80 and CD86 at the protein level. (**e**). Violin plots depict the normalised expression of *CCR9*, *ITGA4* and the transcription factor *POU2AF1* in each defined $CD4^+$ T cell cluster.

Figure 4. Data from independent experiments can be robustly integrated. (**a**) UMAP plot depicts the clustering of resting primary $CD4^+$ T cells from one systemic lupus erythematosus (SLE; n = 9,708 cells) patient, one type 1 diabetes (T1D; n = 7,042 cells) patient and one healthy donor (n = 7,197 cells). Data was integrated from two independent experiments using the same $CD4^+$ T-cell FACS sorting strategy (described in **Fig. 1a**). (**b**) Alignment of the integrated targeted transcriptomics and proteomics data generated from the three assessed donors in two independent experiments. (**c**) UMAP plots depict the donor-specific clustering of the $CD4^+$ T cells. (**d**) Relative proportion of the identified $CD4^+$ T cell clusters in each donor. Frequencies were normalised to either the annotated naïve or memory compartments to ensure higher functional uniformity of the assessed T-cell subsets and to avoid alterations associated with the declining frequency of naïve cells with age. (**e**) Relative expression of the canonical Th1 transcription factor *TBX21* (encoding TBET) and the effector cytokines *NKG7* and *PRF1* on the three assessed donors.

Figure 5. Resting human primary $CD4^+$ T-cells in circulation display variable and modest levels of correlation between mRNA and protein expression at the single-cell level. (**a, b**) Plots depict the correlation (Pearson correlation coefficient) between mRNA and protein expression for 26 markers with concurrent mRNA and protein expression data in resting (**a**) and *in vitro* stimulated (**b**) $CD4^+$ T cells. Correlation was calculated in all $CD4^+$ T cells (blue) or in the $CD45RA^+$ naïve (red) or $CD45RA^-$ memory T-cell subsets separately.

Figure 6. Targeted scRNA-seq and proteomics approach delineates distinct functional subsets in a heterogeneous CD45$^+$ immune cell population isolated from blood and tissue. (**a**) UMAP plot depicts the clustering of the targeted scRNA-seq and transcriptional data of a heterogeneous population of total CD45$^+$ cells isolated from blood and a matched paired duodenal biopsy from two coeliac disease (CD) patients with active disease. (**b**) Sample tag information identifies samples isolated from blood (red) or from the paired duodenal biopsy (teal). (**c, d**) UMAP plot depicting the clustering of the CD45$^+$ cells isolated from blood (**c**) or the paired duodenal biopsy (**d**) from the two CD patients. (**e**) Expression of the CD4 at the protein level (AbSeq) identifies a population of CD4$^+$ T cells in the small intestine. (**f, g**) UMAP plots depict the expression of the regulatory T cell (Treg) transcription factor FOXP3 (**f**), and protein expression (AbSeq) of the three canonical human T follicular helper cells (Tfh) markers, CXCR5, ICOS and PD-1 (**g**) in the CD4$^+$ T cells isolated from tissue. (**h**) Gradient of expression of the Tfh effector genes *IL21*, *CXCL13* and *BTLA* in tissue-resident CD4$^+$ T cells.

Supplement

Supplementary Table 1. FACS and AbSeq anti-human monoclonal antibodies used in this study.

Supplementary Table 2. Summary of the cell capture efficiency and multiplet rates for the experiments performed in this study.

Supplementary Figure legends

Supplementary Figure 1. Protein expression displays much larger dynamic range of expression. (**a, b**) Sequencing saturation metrics of the mRNA (**a**) and protein (**b**) libraries. Saturation of the sequencing libraries was quantified as the number of identified distinct, non-clonally amplified cDNA molecules, marked by a unique molecular identifier (UMI), with increasing sequencing coverage. (**c**) Data shown depicts the distribution (median and range) of the expression of the 42 protein targets measured by AbSeq. Data was derived from the analysis of the first T-cell centric experiment performed on pre-sorted resting $CD4^+$ T cell populations from a systemic lupus erythematosus (SLE) patient.

Supplementary Figure 2. Differential expression in the identified resting and *in vitro* stimulated primary $CD4^+$ T-cell subsets. (**a, b**) Heatmaps depict the top 10 differentially expressed genes in each identified resting (**a**) or *in vitro* stimulated (**b**) $CD4^+$ T-cell clusters. Stimulation condition involved a short period of incubation (90 min) with PMA + ionomycin.

Supplementary Figure 3. *In vitro* stimulation reinforces the trajectories of $CD4^+$ T cell differentiation. (a) UMAP plot depicts the clustering of the *in vitro* stimulated primary $CD4^+$ T cells isolated from blood of a systemic lupus erythematosus (SLE) patient. Stimulation condition involved a short period of incubation (90 min) with PMA + ionomycin. (**b**) Data shown depicts the overlaid protein expression levels of the CD45RA (black to green) and CD45RO (black to red) isoforms in each $CD4^+$ T cell following *in vitro* activation with PMA + ionomycin. (**c, d**) UMAP plots depict the co-expression of the $CD4^+$ T-cell lineage-defining $CD4^+$ Th1 transcription factor TBET and the Th1 effector cytokine IFN-γ (**c**), as well as the Th17 transcription factor RORγt and the Th17 effector cytokine IL-22 (**d**) after *in vitro* stimulation with PMA + ionomycin for 90 min. (**e**) Expression of the canonical Th2 effector molecule IL-13 in *in vitro* stimulated $CD4^+$ T cells. (**f**) UMAP plot depicts the expression of the Treg transcription factor FOXP3 and the prototypical $CD4^+$ Teff cytokine IL-2 in the identified $CD4^+$ T-cell subsets after *in vitro* stimulation with PMA + ionomycin for 90 min. Arrows indicate gradients of expression of the assessed molecules, and indicate the trajectories of $CD4^+$ Th lineage differentiation from naïve cells.

Supplementary Figure 4. Interplay between the BACH2 and BLIMP-1 transcriptional programmes regulate CD4$^+$ Treg activation in humans. (**a**) UMAP plot depicts the expression of the canonical Treg transcription factor FOXP3 in the identified *in vitro* stimulated CD4$^+$ T-cell clusters. (**b**) Data shown depicts the overlaid protein expression levels of the transcription factors BACH2 (black to green) and BLIMP-1 (encoded by *PRDM1*; black to red) in each CD4$^+$ T cell following *in vitro* activation with PMA + ionomycin. (**c**) Heatmap depicts the top 10 differentially expressed genes within the four identified Treg clusters following *in vitro* stimulation with PMA + ionomycin. (**d**) UMAP plots depict the gradient of expression of highly differentially expressed genes in the cluster of activated Tregs (cluster 3) following *in vitro* stimulation with PMA + ionomycin. Red arrows in this figure indicate the gradient of decreasing *BACH2* and concomitant gain in *PRDM1* expression associated with the gradual expression of Treg activation molecules and the acquisition of an activated Treg phenotype.

Supplementary Figure 5. Surface expression of the co-stimulatory molecules CD80 and CD86 marks a subset of highly activated CTLA-4$^+$ human Tregs *in vivo*. (**a,b**) UMAP plots depict the mRNA expression levels of the co-stimulatory molecules CD80 and CD86 in the identified CD4+ T-cell subsets in resting (**a**) and in vitro stimulated (**b**) conditions. Dashed lines delineate the identified activated Treg clusters. (**c**) Gating strategy for the delineation of the Treg subsets according to the intracellular expression of the canonical Treg markers FOXP3 and HELIOS. (d) Histograms depict the mean fluorescence intensity (MFI) of the CTLA-4 expression in the assessed CD4$^+$ T cell subsets. CTLA-4, CD80 and CD86 immunostaining was performed under three different experimental conditions: (i) Surface immunostaining only (black); (ii) Immunostaining after cell permeabilization and fixation (red); and (iii) Both surface immunostaining and after cell permeabilization and fixation. (**e**) Dot plots depict the co-expression of CTLA-4 and CD86 in CD45RA$^-$ CD127^{low}CD25$^+$ Tregs (mTregs) and in the HELIOS-FOXP3$^+$ mTregs. Flow cytometric data was generated from the intracellular immunostaining of CTLA-4 and CD86. (**f,g**) Two dimensional plots depicting the co-expression of CTLA-4 and CD80 (**f**) and HLA-DR and CD86 (**g**) in mTregs. Flow cytometric data was generated from the intracellular immunostaining of the assessed markers. (**h**) Dot plots depict the co-expression between CTLA-4 and either CD80 or CD86 obtained from the surface

immunostaining of these proteins in the mTreg subset. Data shown in this figure was generated from two healthy donors recruited from the Oxford Biobank, depicted in red (freshly isolated PBMCs) and blue (cryopreserved PBMCs), respectively. Cell frequencies from the respective donor are also indicated for each assessed population.

Supplementary Figure 6. Targeted multi-omics approach reveals trajectories of B cell differentiation and class switching in blood and tissue. (**a**) UMAP plots depict the clustering of the total $CD45^+$ immune cells isolated from blood of two coeliac disease (CD) patients with active disease. Dashed lines outline the annotated B-cell and plasma cell subsets annotated from the differentially expressed genes in those clusters. (**b, c**) Expression of key B-cell differentiation and class switching (**b**) and plasma cell (**c**) markers, including *CD27* mRNA and selected surface expressed or secreted immunoglobulin (Ig) receptors in the identified circulating B-cell and plasma cell clusters. (**d**) UMAP plots depict the clustering of the total $CD45^+$ immune cells isolated from duodenal tissue biopsies. Dashed lines outline the annotated B-cell and plasma cell subsets annotated from the differentially expressed genes in those clusters. (**e, f**) Expression of key B-cell differentiation and class switching (**e**) and plasma cell (**f**) markers, including *CD27* mRNA and selected surface expressed or secreted immunoglobulin (Ig) receptors in the identified in the tissue-resident B-cell and plasma cell clusters.

Supplementary Figure 7. Single-cell mRNA and protein quantification identifies distinct functional populations of human circulating $CD3^+$ T cells. (**a**) UMAP plot depicts the clustering of circulating $CD3^+$ T cells isolated from blood of two CD patients with active disease. (**b**) Annotation of the circulating T-cell subsets using the expression profile of CD45RA and additional key lineage defining T-cell markers such as CD4, CD8, *TRDC*, DPP4 and the effector cytokine gene *NKG7*. (**c**) Heatmap depicts the top 10 differentially expressed genes in each identified circulating $CD3^+$ T-cell cluster.

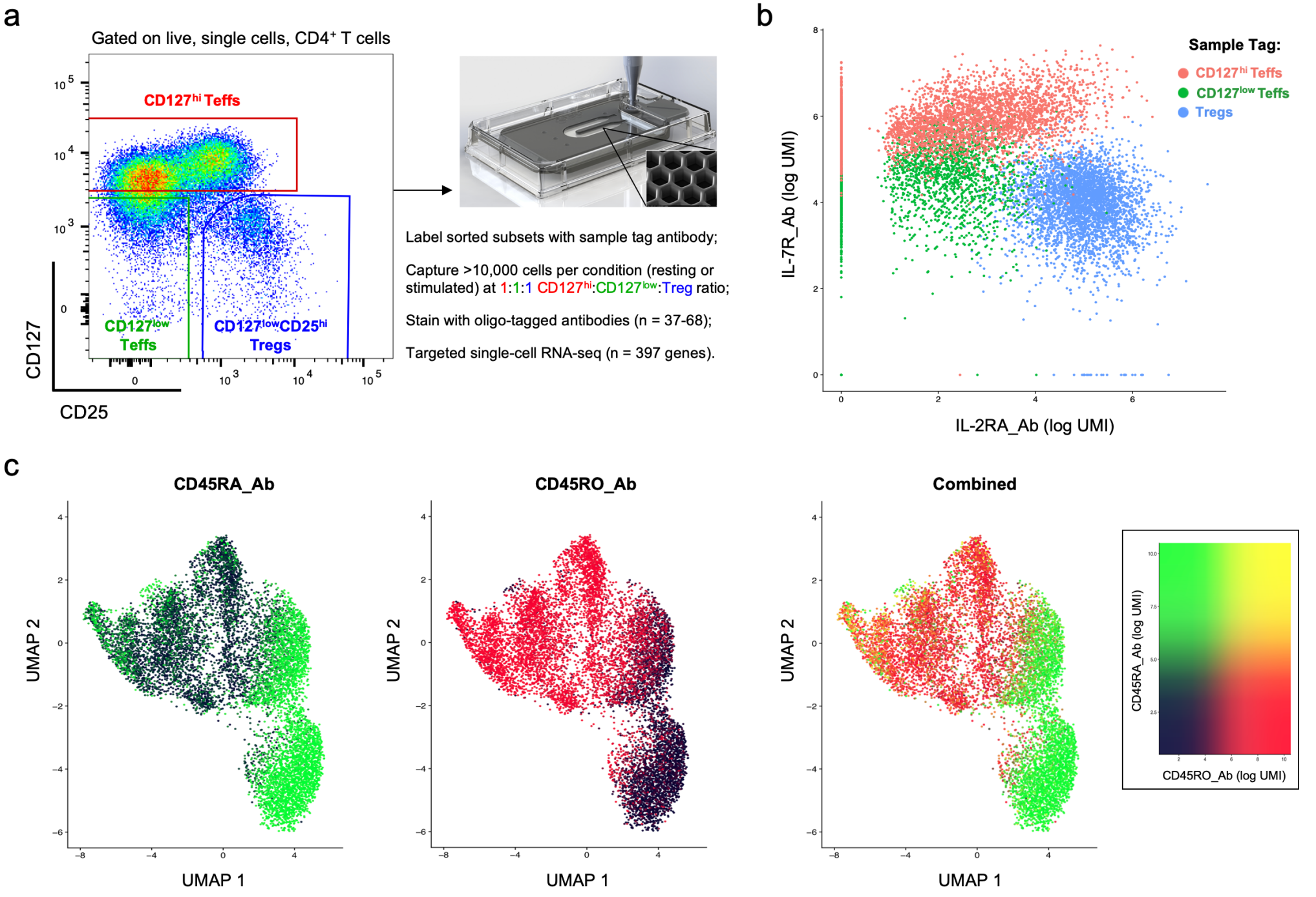
a
Gated on live, single cells, CD4+ T cells
CD127hi Teffs
CD127low Teffs
CD127lowCD25hi Tregs
CD127
CD25
Label sorted subsets with sample tag antibody;
Capture >10,000 cells per condition (resting or stimulated) at 1:1:1 CD127hi:CD127low:Treg ratio;
Stain with oligo-tagged antibodies (n = 37-68);
Targeted single-cell RNA-seq (n = 397 genes).
b
Sample Tag:
CD127hi Teffs
CD127low Teffs
Tregs
IL-7R_Ab (log UMI)
IL-2RA_Ab (log UMI)
c
CD45RA_Ab
CD45RO_Ab
Combined
UMAP 2
UMAP 1
CD45RA_Ab (log UMI)
CD45RO_Ab (log UMI)

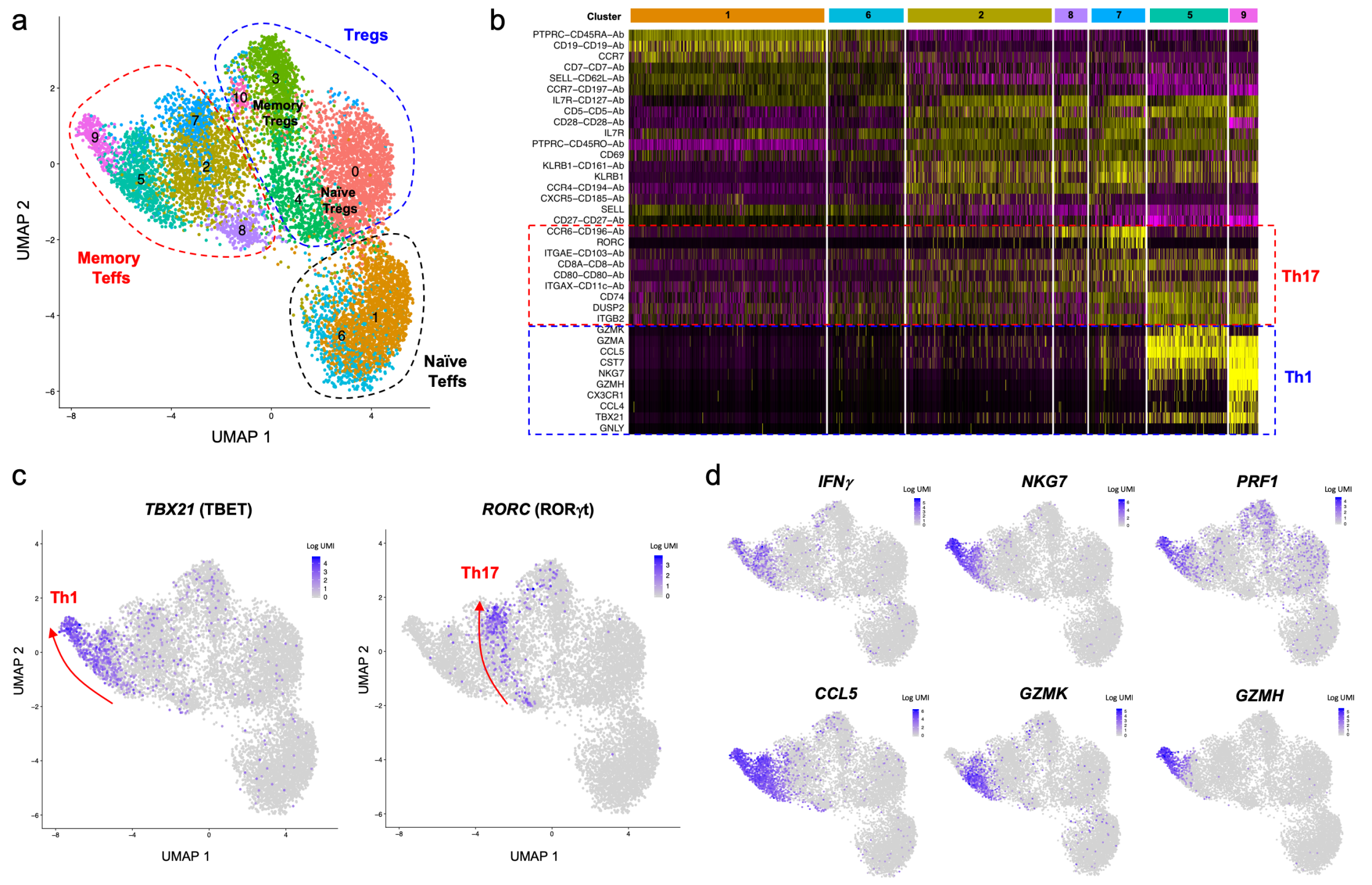
a
Tregs
Memory Tregs
Naïve Tregs
Memory Teffs
Naïve Teffs
UMAP 1
UMAP 2
b
Cluster
1
6
2
8
7
5
9
PTPRC−CD45RA−Ab
CD19−CD19−Ab
CCR7
CD7−CD7−Ab
SELL−CD62L−Ab
CCR7−CD197−Ab
IL7R−CD127−Ab
CD5−CD5−Ab
CD28−CD28−Ab
IL7R
PTPRC−CD45RO−Ab
CD69
KLRB1−CD161−Ab
KLRB1
CCR4−CD194−Ab
CXCR5−CD185−Ab
SELL
CD27−CD27−Ab
CCR6−CD196−Ab
RORC
ITGAE−CD103−Ab
CD8A−CD8−Ab
CD80−CD80−Ab
ITGAX−CD11c−Ab
CD74
DUSP2
ITGB2
GZMK
GZMA
CCL5
CST7
NKG7
GZMH
CX3CR1
CCL4
TBX21
GNLY
Th17
Th1
c
TBX21 (TBET)
RORC (RORγt)
Th1
Th17
Log UMI
UMAP 1
UMAP 2
d
IFNγ
NKG7
PRF1
CCL5
GZMK
GZMH
Log UMI

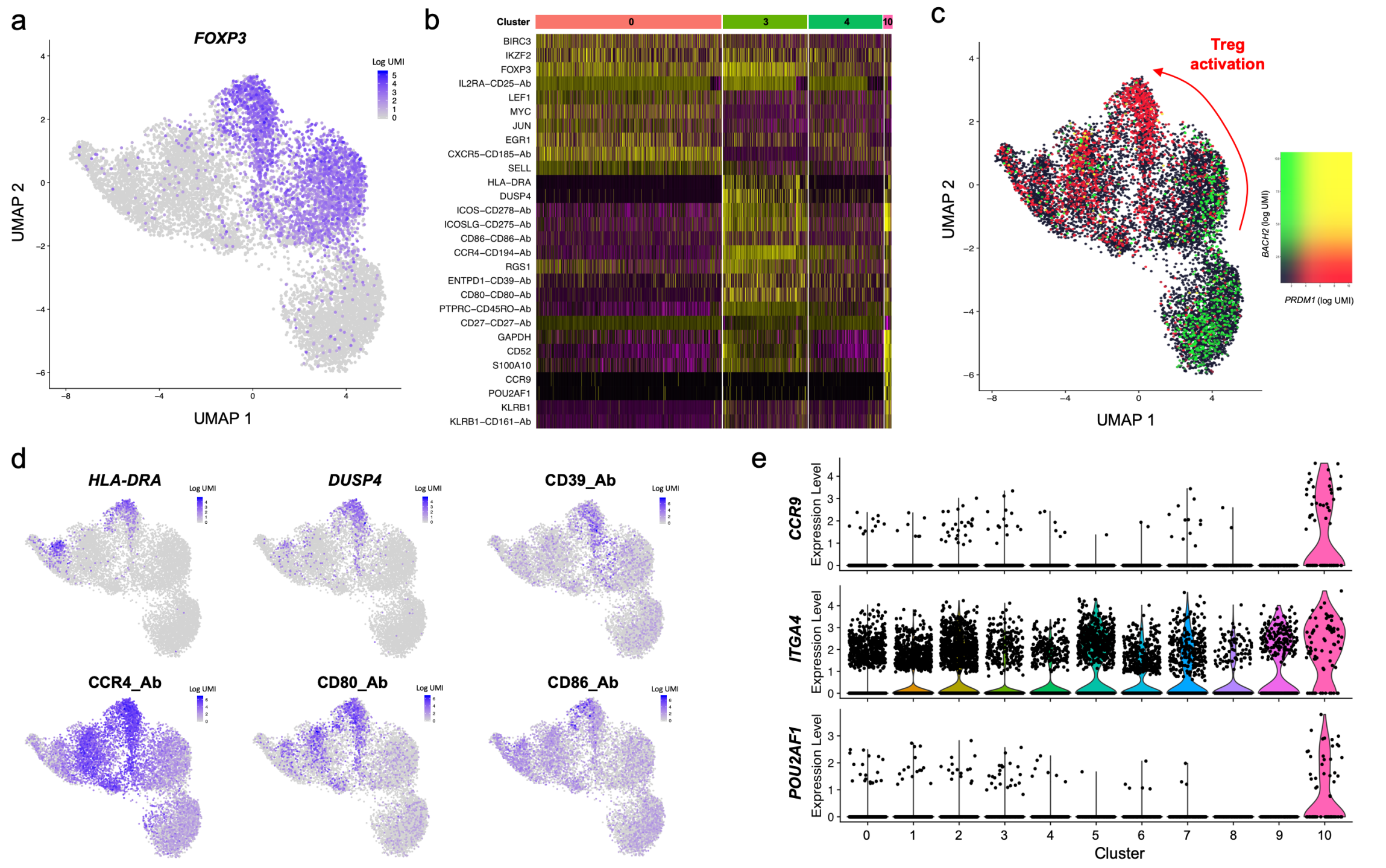
a
FOXP3
Log UMI
UMAP 2
UMAP 1
b
Cluster
0
3
4
10
BIRC3
IKZF2
FOXP3
IL2RA–CD25–Ab
LEF1
MYC
JUN
EGR1
CXCR5–CD185–Ab
SELL
HLA–DRA
DUSP4
ICOS–CD278–Ab
ICOSLG–CD275–Ab
CD86–CD86–Ab
CCR4–CD194–Ab
RGS1
ENTPD1–CD39–Ab
CD80–CD80–Ab
PTPRC–CD45RO–Ab
CD27–CD27–Ab
GAPDH
CD52
S100A10
CCR9
POU2AF1
KLRB1
KLRB1–CD161–Ab
c
Treg activation
BACH2 (log UMI)
PRDM1 (log UMI)
UMAP 2
UMAP 1
d
HLA-DRA
DUSP4
CD39_Ab
CCR4_Ab
CD80_Ab
CD86_Ab
Log UMI
e
CCR9
ITGA4
POU2AF1
Expression Level
Cluster

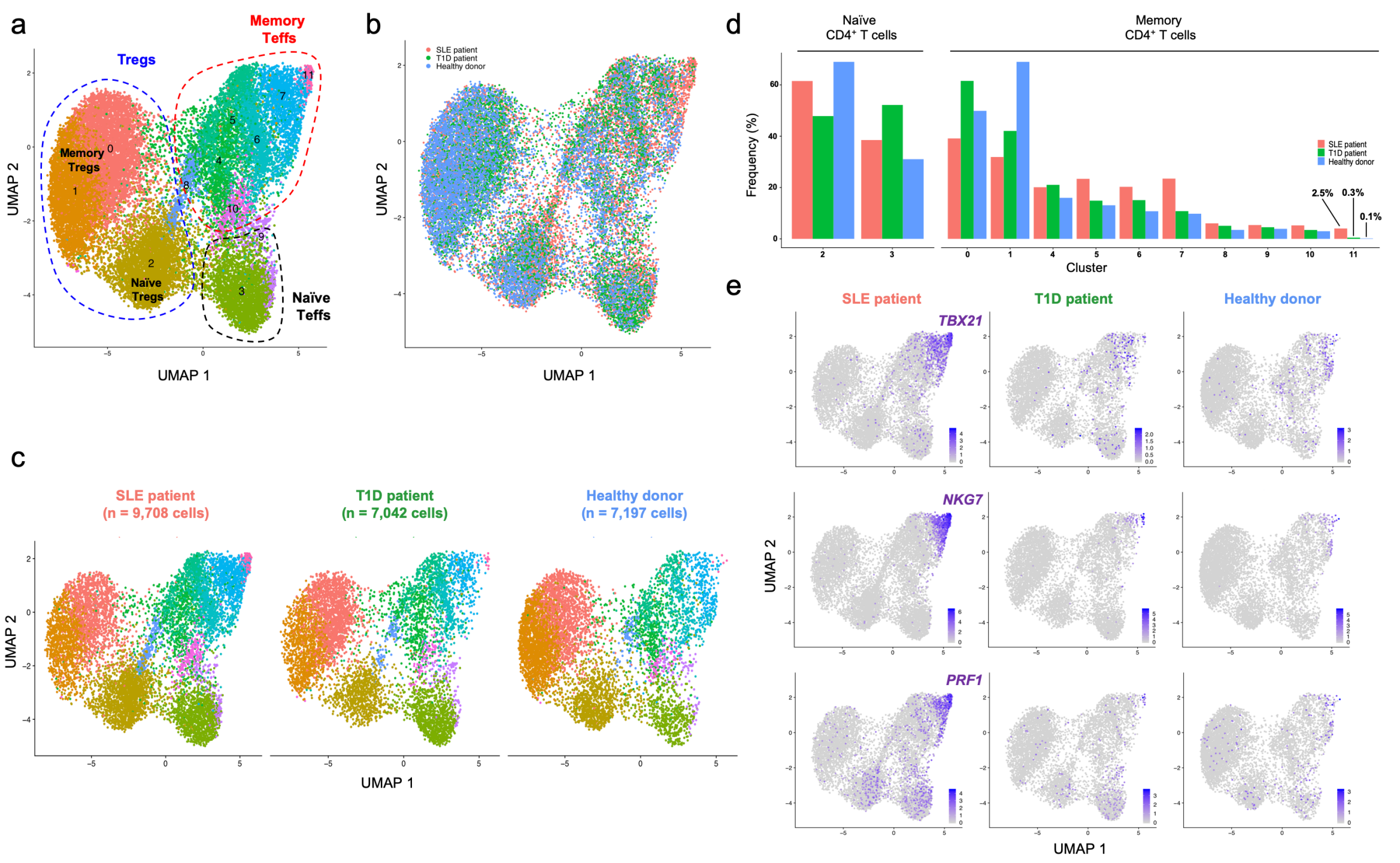
a
Memory Teffs
Tregs
Memory Tregs
Naïve Tregs
Naïve Teffs
UMAP 2
UMAP 1
b
SLE patient
T1D patient
Healthy donor
UMAP 2
UMAP 1
c
SLE patient (n = 9,708 cells)
T1D patient (n = 7,042 cells)
Healthy donor (n = 7,197 cells)
UMAP 2
UMAP 1
d
Naïve CD4+ T cells
Memory CD4+ T cells
Frequency (%)
Cluster
SLE patient
T1D patient
Healthy donor
2.5%
0.3%
0.1%
e
SLE patient
T1D patient
Healthy donor
TBX21
NKG7
PRF1
UMAP 2
UMAP 1

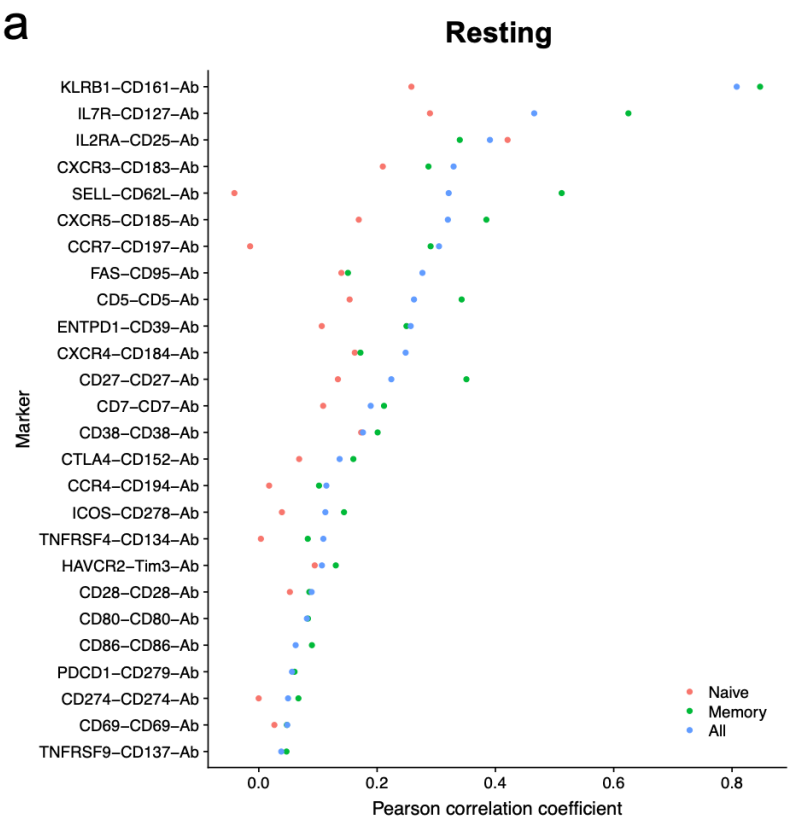
a
Resting
KLRB1–CD161–Ab
IL7R–CD127–Ab
IL2RA–CD25–Ab
CXCR3–CD183–Ab
SELL–CD62L–Ab
CXCR5–CD185–Ab
CCR7–CD197–Ab
FAS–CD95–Ab
CD5–CD5–Ab
ENTPD1–CD39–Ab
CXCR4–CD184–Ab
CD27–CD27–Ab
CD7–CD7–Ab
CD38–CD38–Ab
CTLA4–CD152–Ab
CCR4–CD194–Ab
ICOS–CD278–Ab
TNFRSF4–CD134–Ab
HAVCR2–Tim3–Ab
CD28–CD28–Ab
CD80–CD80–Ab
CD86–CD86–Ab
PDCD1–CD279–Ab
CD274–CD274–Ab
CD69–CD69–Ab
TNFRSF9–CD137–Ab
Marker
0.0
0.2
0.4
0.6
0.8
Pearson correlation coefficient
Naive
Memory
All

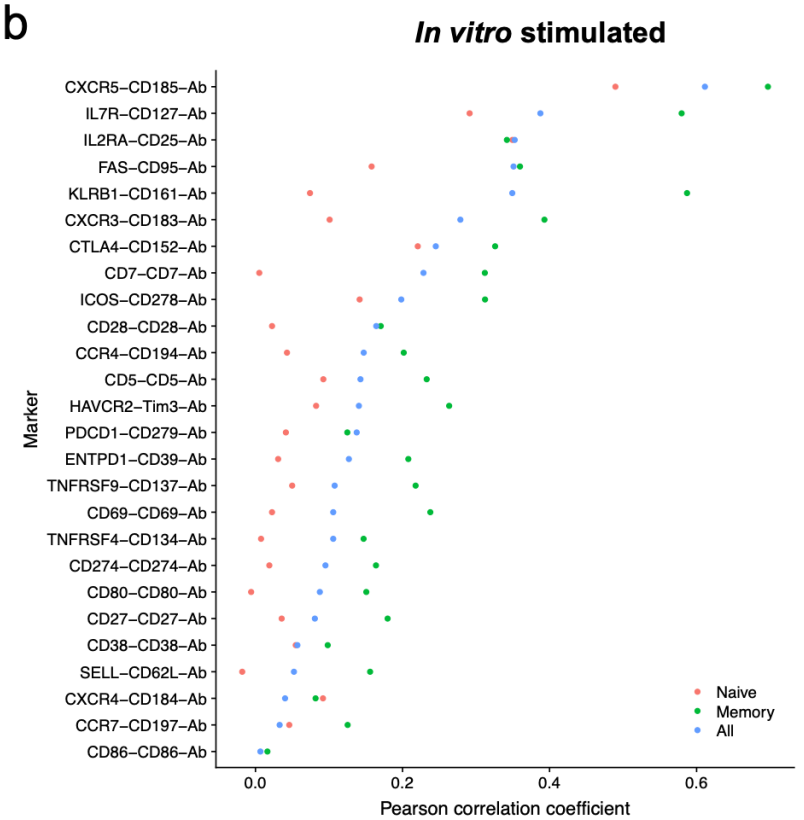
b
In vitro stimulated
CXCR5–CD185–Ab
IL7R–CD127–Ab
IL2RA–CD25–Ab
FAS–CD95–Ab
KLRB1–CD161–Ab
CXCR3–CD183–Ab
CTLA4–CD152–Ab
CD7–CD7–Ab
ICOS–CD278–Ab
CD28–CD28–Ab
CCR4–CD194–Ab
CD5–CD5–Ab
HAVCR2–Tim3–Ab
PDCD1–CD279–Ab
ENTPD1–CD39–Ab
TNFRSF9–CD137–Ab
CD69–CD69–Ab
TNFRSF4–CD134–Ab
CD274–CD274–Ab
CD80–CD80–Ab
CD27–CD27–Ab
CD38–CD38–Ab
SELL–CD62L–Ab
CXCR4–CD184–Ab
CCR7–CD197–Ab
CD86–CD86–Ab
Marker
0.0
0.2
0.4
0.6
Pearson correlation coefficient
Naive
Memory
All

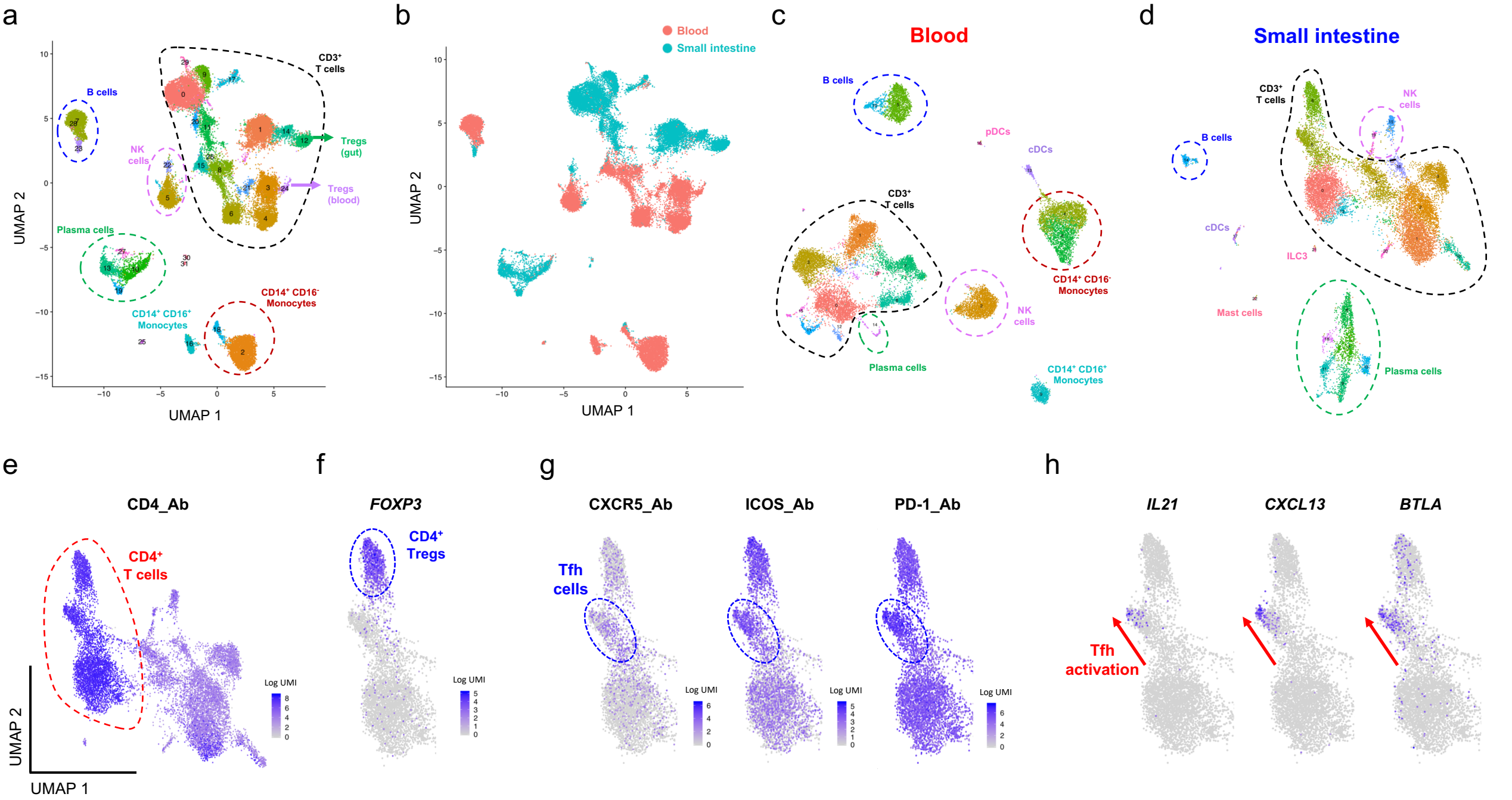
a
CD3+ T cells
B cells
NK cells
Tregs (gut)
Tregs (blood)
Plasma cells
CD14+ CD16- Monocytes
CD14+ CD16+ Monocytes
UMAP 2
UMAP 1
b
Blood
Small intestine
UMAP 2
UMAP 1
c
Blood
B cells
pDCs
cDCs
CD3+ T cells
CD14+ CD16- Monocytes
NK cells
Plasma cells
CD14+ CD16+ Monocytes
d
Small intestine
CD3+ T cells
NK cells
B cells
cDCs
ILC3
Mast cells
Plasma cells
e
CD4_Ab
CD4+ T cells
Log UMI
UMAP 2
UMAP 1
f
FOXP3
CD4+ Tregs
Log UMI
g
CXCR5_Ab
ICOS_Ab
PD-1_Ab
Tfh cells
Log UMI
h
IL21
CXCL13
BTLA
Tfh activation

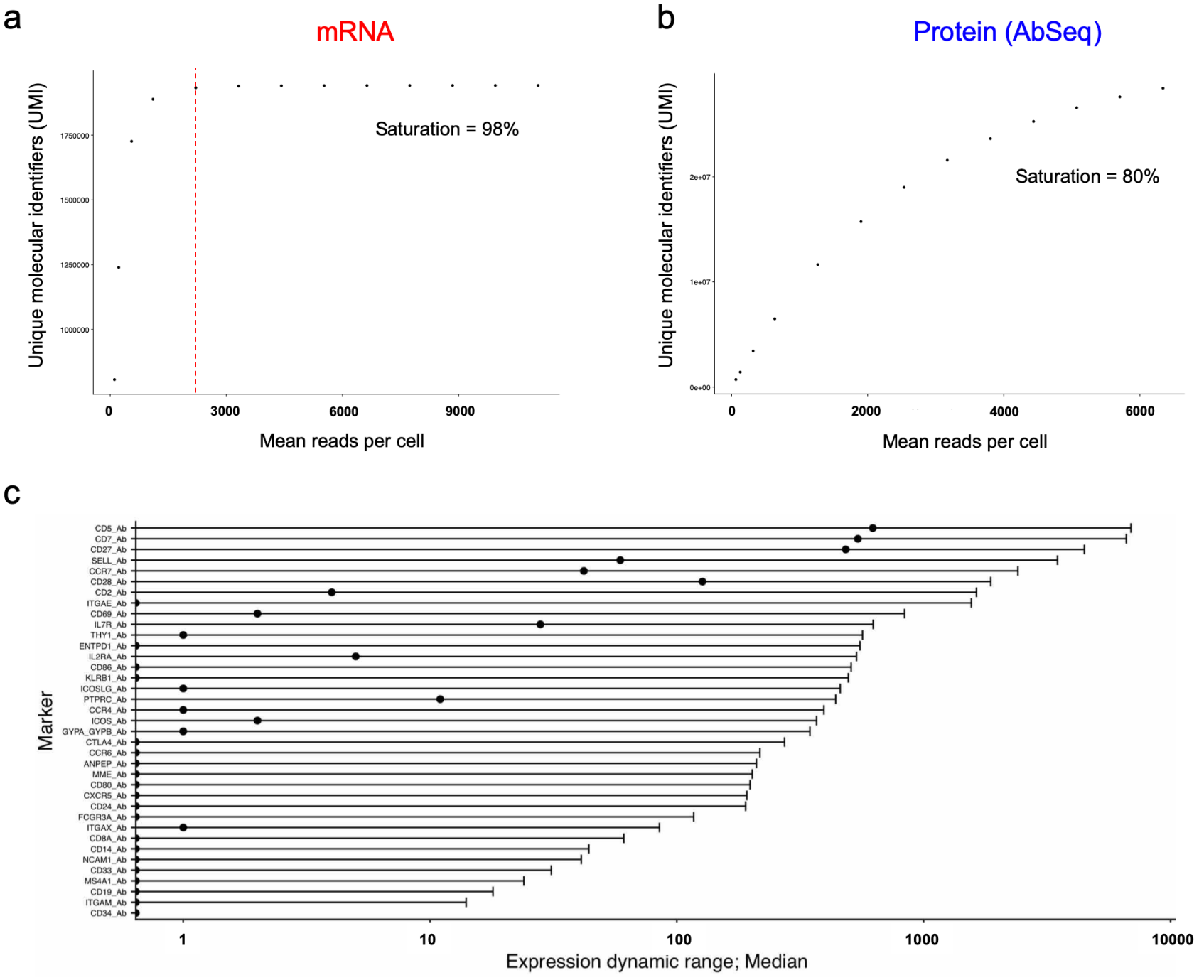
a
mRNA
Unique molecular identifiers (UMI)
1750000
1500000
1250000
1000000
Saturation = 98%
0
3000
6000
9000
Mean reads per cell
b
Protein (AbSeq)
Unique molecular identifiers (UMI)
2e+07
1e+07
0e+00
Saturation = 80%
0
2000
4000
6000
Mean reads per cell
c
Marker
CD5_Ab
CD7_Ab
CD27_Ab
SELL_Ab
CCR7_Ab
CD28_Ab
CD2_Ab
ITGAE_Ab
CD69_Ab
IL7R_Ab
THY1_Ab
ENTPD1_Ab
IL2RA_Ab
CD86_Ab
KLRB1_Ab
ICOSLG_Ab
PTPRC_Ab
CCR4_Ab
ICOS_Ab
GYPA_GYPB_Ab
CTLA4_Ab
CCR6_Ab
ANPEP_Ab
MME_Ab
CD80_Ab
CXCR5_Ab
CD24_Ab
FCGR3A_Ab
ITGAX_Ab
CD8A_Ab
CD14_Ab
NCAM1_Ab
CD33_Ab
MS4A1_Ab
CD19_Ab
ITGAM_Ab
CD34_Ab
1
10
100
1000
10000
Expression dynamic range; Median

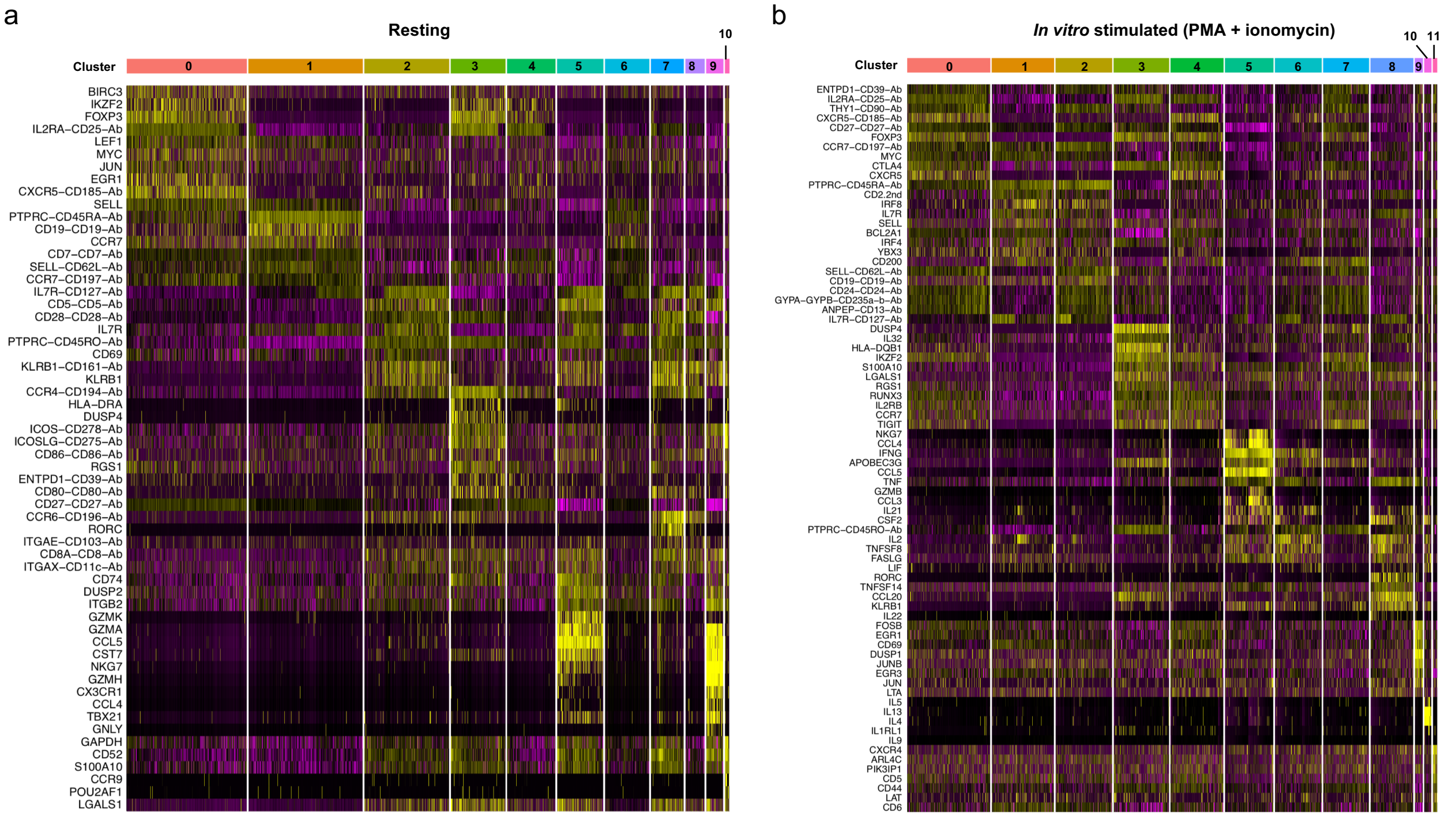
a
Resting
Cluster
0
1
2
3
4
5
6
7
8
9
10
BIRC3
IKZF2
FOXP3
IL2RA–CD25–Ab
LEF1
MYC
JUN
EGR1
CXCR5–CD185–Ab
SELL
PTPRC–CD45RA–Ab
CD19–CD19–Ab
CCR7
CD7–CD7–Ab
SELL–CD62L–Ab
CCR7–CD197–Ab
IL7R–CD127–Ab
CD5–CD5–Ab
CD28–CD28–Ab
IL7R
PTPRC–CD45RO–Ab
CD69
KLRB1–CD161–Ab
KLRB1
CCR4–CD194–Ab
HLA–DRA
DUSP4
ICOS–CD278–Ab
ICOSLG–CD275–Ab
CD86–CD86–Ab
RGS1
ENTPD1–CD39–Ab
CD80–CD80–Ab
CD27–CD27–Ab
CCR6–CD196–Ab
RORC
ITGAE–CD103–Ab
CD8A–CD8–Ab
ITGAX–CD11c–Ab
CD74
DUSP2
ITGB2
GZMK
GZMA
CCL5
CST7
NKG7
GZMH
CX3CR1
CCL4
TBX21
GNLY
GAPDH
CD52
S100A10
CCR9
POU2AF1
LGALS1
b
In vitro stimulated (PMA + ionomycin)
Cluster
0
1
2
3
4
5
6
7
8
9
10
11
ENTPD1–CD39–Ab
IL2RA–CD25–Ab
THY1–CD90–Ab
CXCR5–CD185–Ab
CD27–CD27–Ab
FOXP3
CCR7–CD197–Ab
MYC
CTLA4
CXCR5
PTPRC–CD45RA–Ab
CD2.2nd
IRF8
IL7R
SELL
BCL2A1
IRF4
YBX3
CD200
SELL–CD62L–Ab
CD19–CD19–Ab
CD24–CD24–Ab
GYPA–GYPB–CD235a–b–Ab
ANPEP–CD13–Ab
IL7R–CD127–Ab
DUSP4
IL32
HLA–DQB1
IKZF2
S100A10
LGALS1
RGS1
RUNX3
IL2RB
CCR7
TIGIT
NKG7
CCL4
IFNG
APOBEC3G
CCL5
TNF
GZMB
CCL3
IL21
CSF2
PTPRC–CD45RO–Ab
IL2
TNFSF8
FASLG
LIF
RORC
TNFSF14
CCL20
KLRB1
IL22
FOSB
EGR1
CD69
DUSP1
JUNB
EGR3
JUN
LTA
IL5
IL13
IL4
IL1RL1
IL9
CXCR4
ARL4C
PIK3IP1
CD5
CD44
LAT
CD6

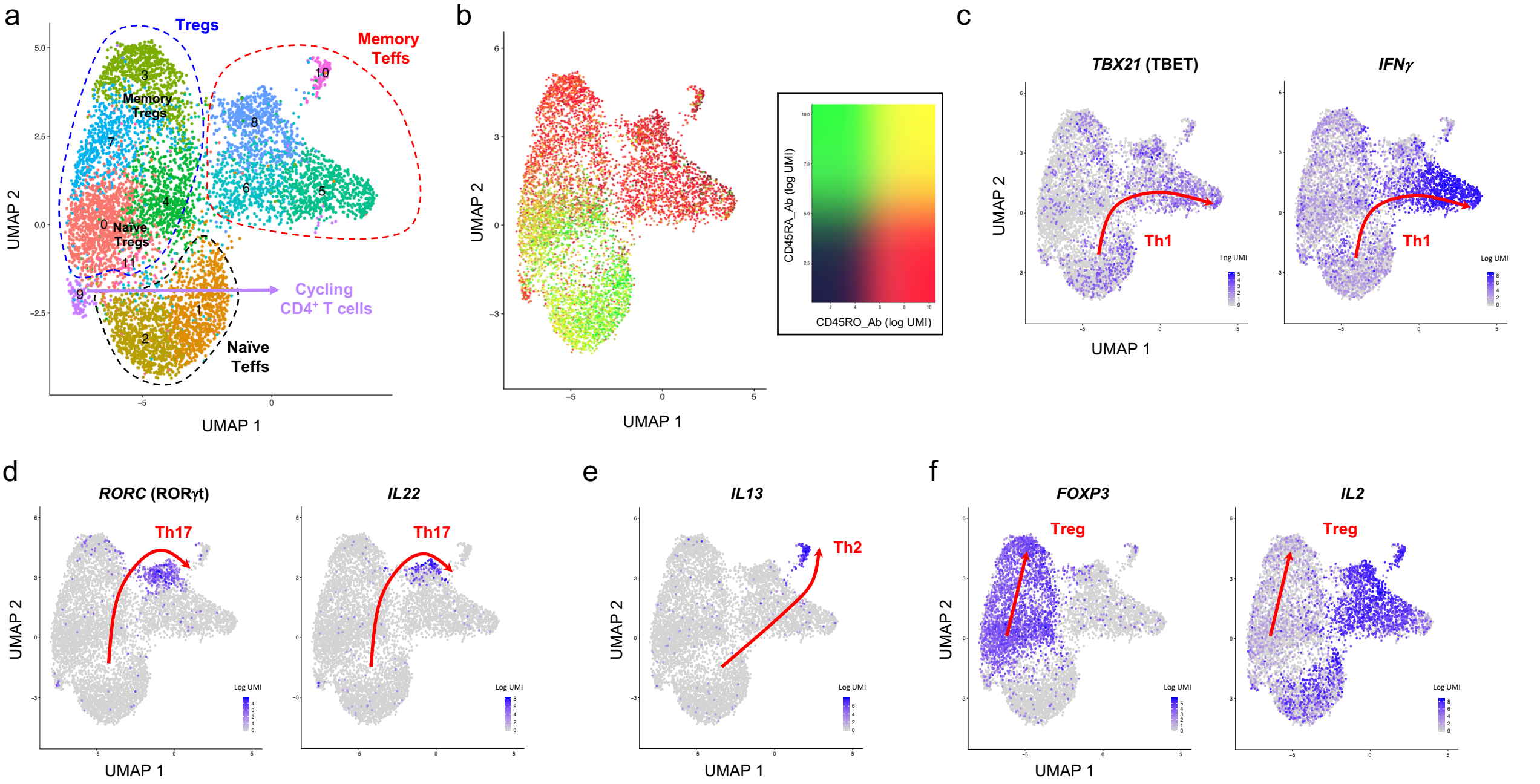
a
Tregs
Memory Teffs
Memory Tregs
Naïve Tregs
Cycling CD4+ T cells
Naïve Teffs
UMAP 2
UMAP 1
b
CD45RA_Ab (log UMI)
CD45RO_Ab (log UMI)
UMAP 2
UMAP 1
c
TBX21 (TBET)
IFNγ
Th1
Log UMI
UMAP 2
UMAP 1
d
RORC (RORγt)
IL22
Th17
Log UMI
UMAP 2
UMAP 1
e
IL13
Th2
Log UMI
UMAP 2
UMAP 1
f
FOXP3
IL2
Treg
Log UMI
UMAP 2
UMAP 1

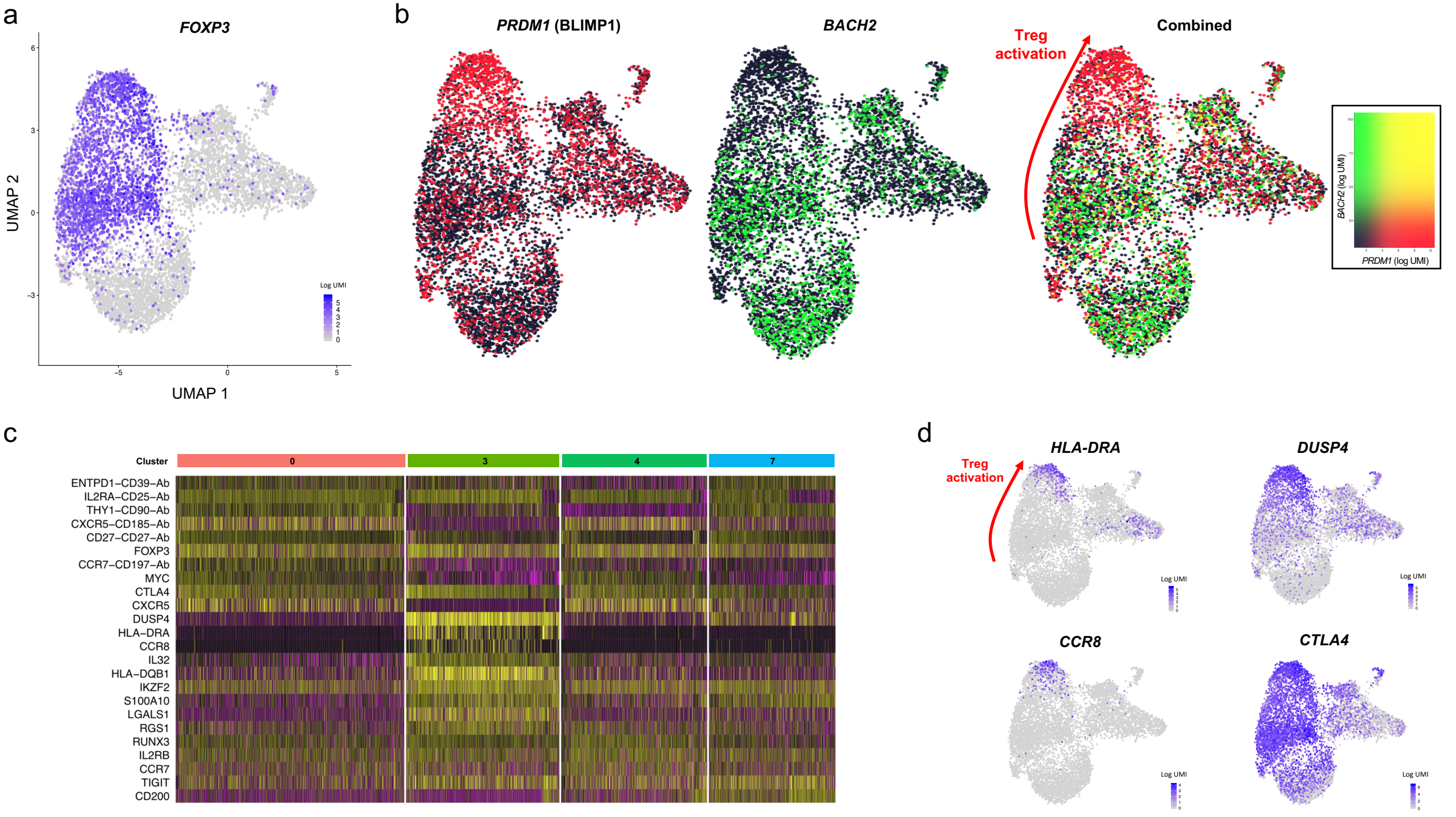
a
FOXP3
UMAP 2
UMAP 1
Log UMI
b
PRDM1 (BLIMP1)
BACH2
Combined
Treg activation
BACH2 (log UMI)
PRDM1 (log UMI)
c
Cluster
0
3
4
7
ENTPD1–CD39–Ab
IL2RA–CD25–Ab
THY1–CD90–Ab
CXCR5–CD185–Ab
CD27–CD27–Ab
FOXP3
CCR7–CD197–Ab
MYC
CTLA4
CXCR5
DUSP4
HLA–DRA
CCR8
IL32
HLA–DQB1
IKZF2
S100A10
LGALS1
RGS1
RUNX3
IL2RB
CCR7
TIGIT
CD200
d
HLA-DRA
DUSP4
CCR8
CTLA4
Treg activation
Log UMI

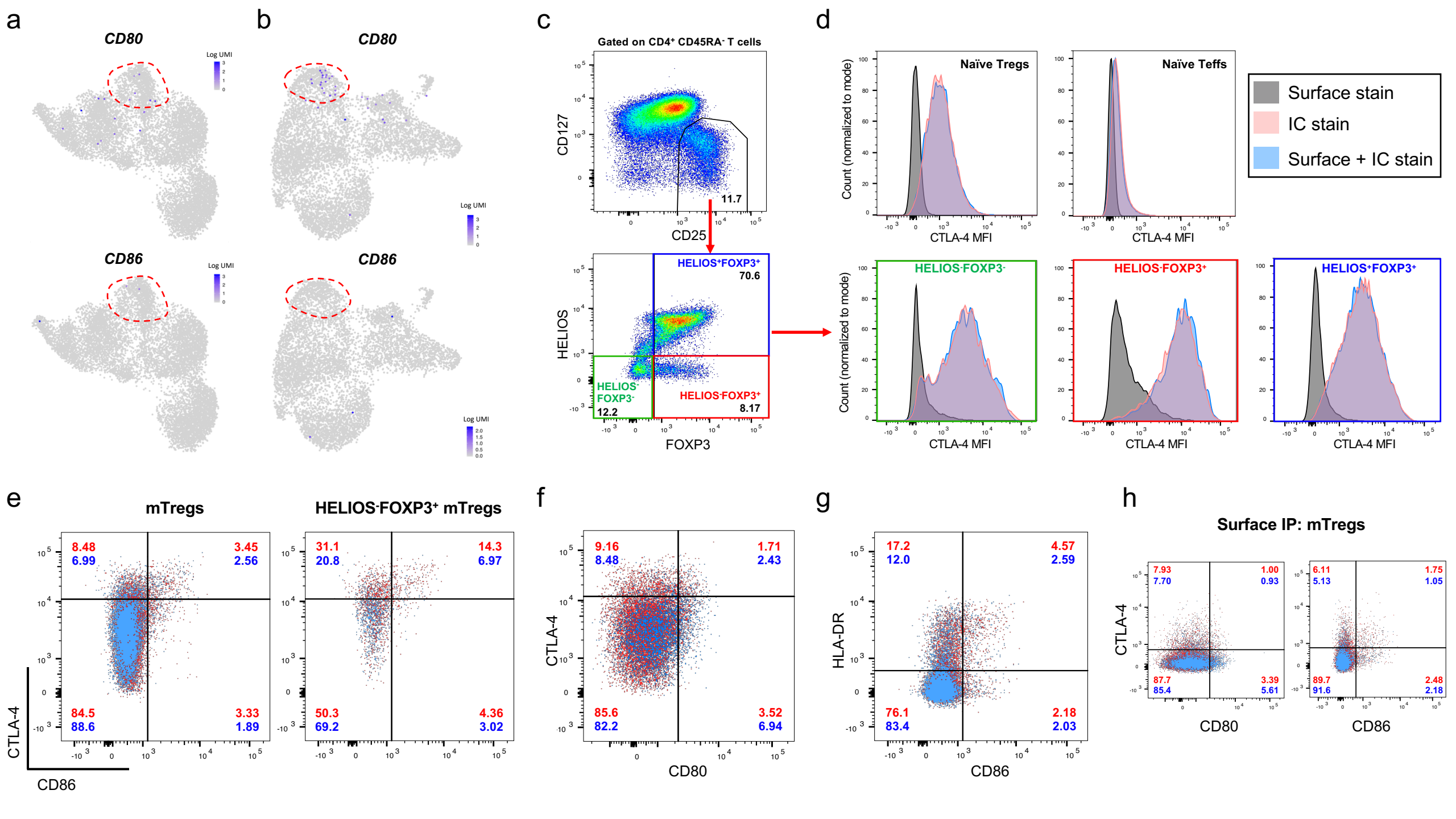
a
CD80
Log UMI
CD86
b
CD80
Log UMI
CD86
Log UMI
c
Gated on CD4+ CD45RA- T cells
CD127
CD25
11.7
HELIOS
FOXP3
HELIOS+FOXP3+
70.6
HELIOS-FOXP3-
12.2
HELIOS-FOXP3+
8.17
d
Naïve Tregs
Naïve Teffs
Count (normalized to mode)
CTLA-4 MFI
Surface stain
IC stain
Surface + IC stain
HELIOS-FOXP3-
HELIOS-FOXP3+
HELIOS+FOXP3+
e
mTregs
HELIOS-FOXP3+ mTregs
CTLA-4
CD86
8.48
6.99
3.45
2.56
84.5
88.6
3.33
1.89
31.1
20.8
14.3
6.97
50.3
69.2
4.36
3.02
f
CTLA-4
CD80
9.16
8.48
1.71
2.43
85.6
82.2
3.52
6.94
g
HLA-DR
CD86
17.2
12.0
4.57
2.59
76.1
83.4
2.18
2.03
h
Surface IP: mTregs
CTLA-4
CD80
CD86
7.93
7.70
1.00
0.93
87.7
85.4
3.39
5.61
6.11
5.13
1.75
1.05
89.7
91.6
2.48
2.18

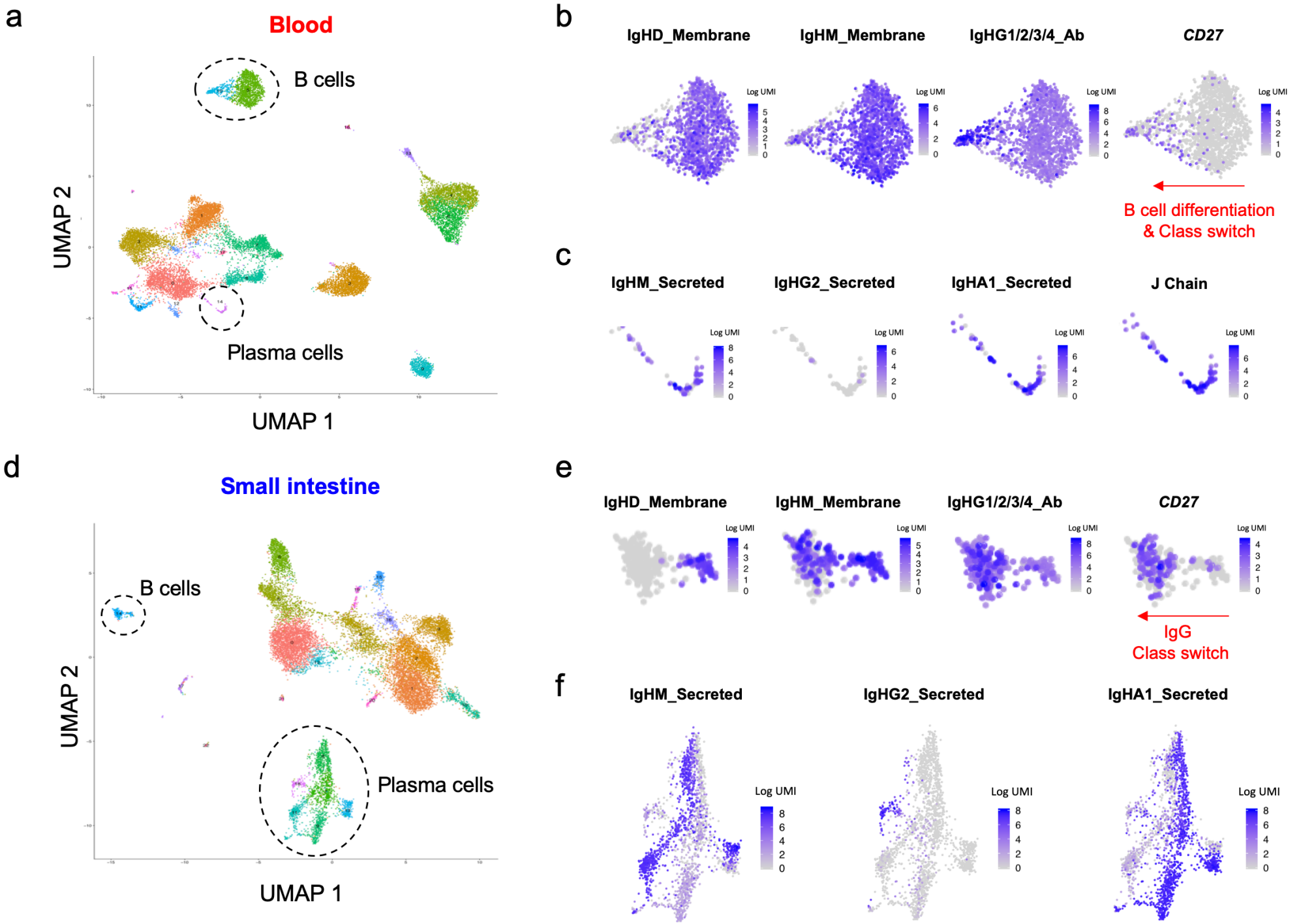
a
Blood
B cells
Plasma cells
UMAP 2
UMAP 1
b
IgHD_Membrane
IgHM_Membrane
IgHG1/2/3/4_Ab
CD27
Log UMI
B cell differentiation
& Class switch
c
IgHM_Secreted
IgHG2_Secreted
IgHA1_Secreted
J Chain
d
Small intestine
B cells
Plasma cells
UMAP 2
UMAP 1
e
IgHD_Membrane
IgHM_Membrane
IgHG1/2/3/4_Ab
CD27
IgG
Class switch
f
IgHM_Secreted
IgHG2_Secreted
IgHA1_Secreted

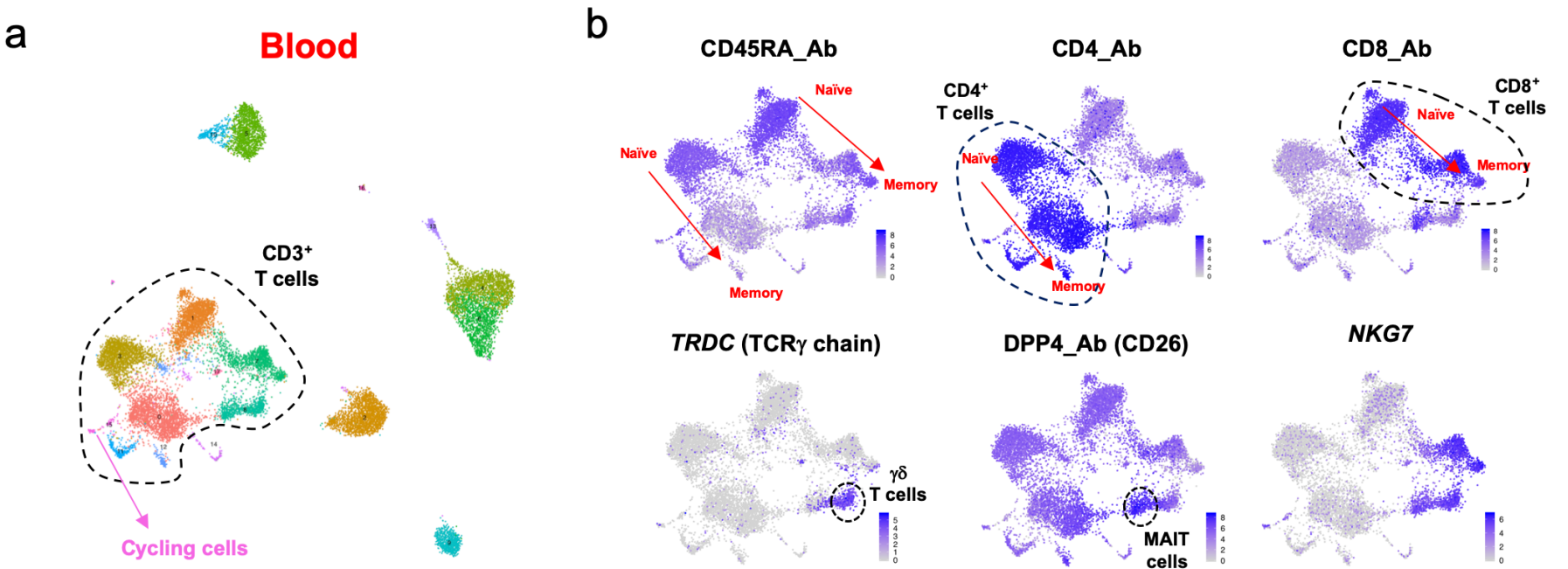
a
Blood
CD3+
T cells
Cycling cells
b
CD45RA_Ab
Naïve
Memory
Naïve
Memory
CD4_Ab
CD4+
T cells
Naïve
Memory
CD8_Ab
CD8+
T cells
Naïve
Memory
TRDC (TCRγ chain)
γδ
T cells
DPP4_Ab (CD26)
MAIT
cells
NKG7